

Application of local gauge theory to fluid mechanics

Part II

Example: Basic model of Tollmien-Schlichting waves and analytical solution

Thomas Merz

8055 Zürich, CH, e-mail: t.merz@alumni.ethz.ch

June 2023

Abstract. The gauge field equation for fluid mechanics established in Part I is developed into a first-order scattering theory in the simplified case of a two-dimensional incompressible flow over a flat plate. This is used to present a model for the origin of Tollmien-Schlichting (TS) waves based on scattering between fluid particles.

As a result, analytical formulae for the maximum amplification factor and the transition point from laminar to turbulent flow in the boundary layer are obtained. The mathematical transformations from the stationary field equations in Part I to a scattering theory with time evolution along the flow axis using Wick rotation are elaborated in detail.

Keywords: fundamental fluid mechanics, turbulence, gauge theories and their applications

1 Introduction

1.1 *Current state, goal and further procedure*

In the first part, a gauge field equation was presented by Eq. 71 from which the Navier-Stokes equations (NS equations) can be derived. It was shown that this equation contains the information of the stationary NS equations up to a similarity transformation. In addition, it was demonstrated that an interpretation of the gauge fields as convective components of the velocity field of a fluid is possible.

The goal of the second part is to advance this gauge field equation into an operational scattering theory and to demonstrate how it can be applied in practice through an example.

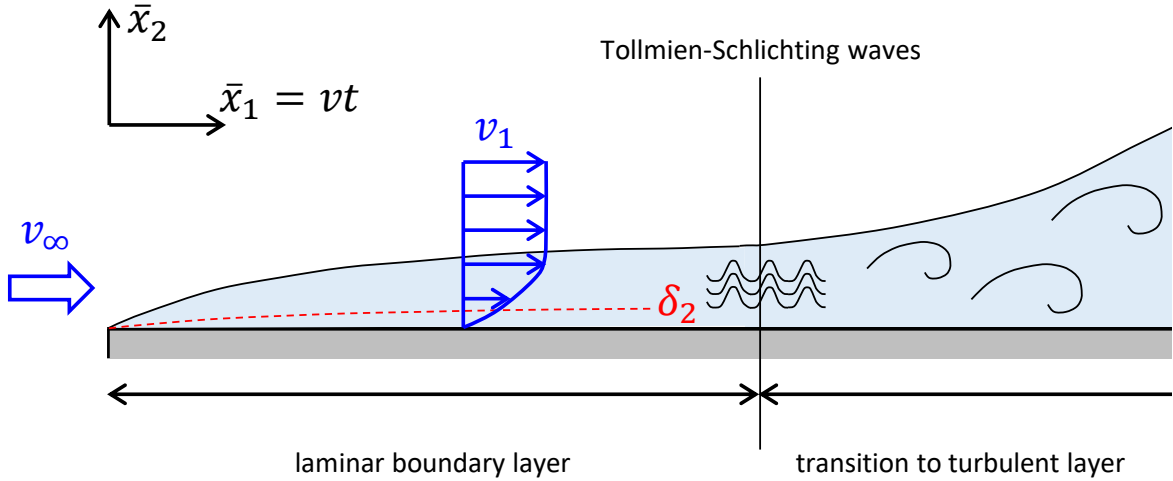


Figure 1: Schematic illustration of a boundary layer flow (light blue) over a flat plate (gray). A flow with velocity v_∞ hits a plate from the left. The flow decelerates above the plate to the laminar velocity profile v_1 (blue arrows) with the momentum thickness δ_2 (red) plotted. Downstream, the transition to a turbulent boundary layer occurs, starting with characteristic wave-like flow patterns, the Tollmien-Schlichting (TS) waves.

For this purpose, building on the field equation from Part I, a quantized view is introduced, describing the fluid consisting of quasiparticles possessing purely laminar or purely vortical properties. From this description, a scattering theory of the fluid quasiparticles among themselves is developed.

This approach is used to study the formation of Tollmien-Schlichting (TS) waves: Wavelike structures arising in the two-dimensional airflow over a flat plate or wing profile, marking the first visible step of the transition from laminar to turbulent flow in the boundary layer (Fig. 1). This transition point has a high relevance in the optimization of airfoils and is therefore well studied experimentally (Tollmien 1929, Schlichting 1933 as well as e.g. Schlichting & Gersten 2017 and references therein).

The current models for the theoretical description of TS waves are based on tracking the evolution of perturbations along streamlines over the plate (solution of the Orr-Sommerfeld equation by linear stability theory, e^N -method and similar numerical methods, see e.g. van Ingen 2008, Schmid & Henningson 2012 and references therein). Within an instability zone, the amplitude of the perturbations is amplified. This amplification can be quantified by numerical integration. Reaching a cumulative amplification by a factor of e^N (usually $N = 9$) of the original perturbation is considered as the transition point to TS waves. Two corresponding examples from Simon (2017) are shown in Fig. 2.

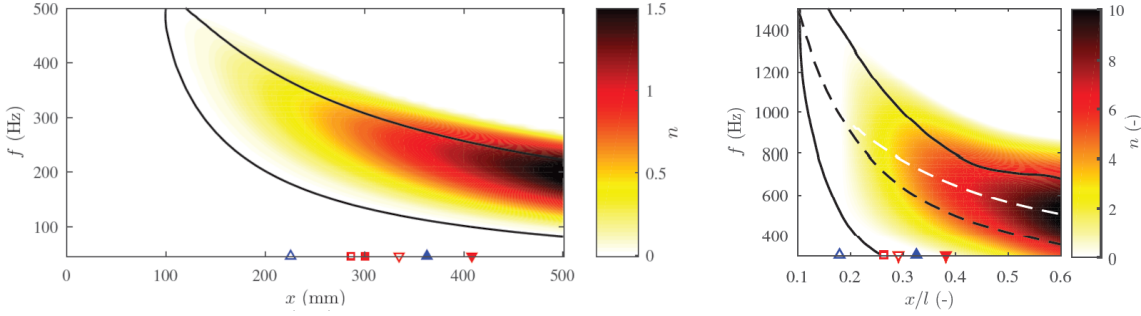


Figure 2: Two examples of frequency-amplification diagrams using the e^N method from Simon (2017). On the left for the situation in a wind tunnel, on the right for a test flight. Within the instability zones, perturbation frequencies are amplified (black line, maximum amplification dashed in black). Integration of the amplification along the x -axis gives the accumulated gain, which is shown logarithmically as amplification factor n from e^n (colored contours yellow-red-black). The maximum accumulated gain e^N (white-dashed line) in the case of the flight example exceeds the transition point to TS waves $N = 9$ in the range of $x/l \approx 0.55$. These data are calculated numerically.

However, the success of these models is limited (van Ingen, 2008): Numerical integration is costly and leads to inaccurate results. In addition, the models are limited to TS waves and are not suitable for characterizing the further transition to turbulence, since the originating problem in describing turbulence is not solved: The key issue in modeling turbulent flows is that the traveled path of a single fluid volume starts behaving chaotically. The concept of the streamline as the path of a single fluid volume thus loses its relevance.

The advantage of the presented approach through a quantized point of view lies in the application of the path integral formalism as it is used in quantum mechanics. This formalism takes into account all possible paths of motion and their probability simultaneously, and as a result brings out those *statistical* aspects which are still valid when it becomes impossible to trace the path of a single fluid volume.

Applied to fluid mechanics, the formalism thus abandons the tracking of individual particles, but in return allows a direct statistical analysis of the overall flow behavior. Further advantages of this approach are:

- An analytical result is obtained whereas with the conventional approach only numerical solutions are possible.
- The model as a scattering theory provides an explanatory approach for the emergence of turbulence based on elementary physical principles.
- The new approach is extendable to the later stages of the transition to turbulence. By expanding the theory to the three-dimensional case and taking higher order perturbation terms into account, nonlinear effects can be modeled due to self-interaction of the vortex gauge fields.

The proposed model can be split into three steps:

- (i) The undisturbed laminar flow consists of elementary laminar quasiparticles without angular momentum. The magnitude and direction of the undisturbed flow defines, by means of $x_1 = vt$, a basic time axis along which the time evolution of the following processes takes place. This axis is used to introduce a covariant time scale using Wick rotation.
- (ii) The perturbation by the plate causes the creation of elementary vortices of different rotational frequencies at this location. The elementary vortices are bosonic quasiparticles with rotational components whose properties depend on the Reynolds number.
- (iii) The elementary vortices and the laminar quasiparticles subsequently collide and scatter from each other as they move downstream along the plate. Similar to the Compton effect in quantum mechanics, the rotational frequency of the elementary vortices decreases with each scattering process. In this process, high frequencies are reduced more than low ones, leading to the accumulation of elementary vortices with similar frequencies downstream and ultimately to the formation of a resonance, which becomes observable macroscopically.

The further procedure is as follows: In Section 2 the field equation Eq. 71 from Part I is transformed such that it is expressed as similar as possible to existing scattering theories, and the fields get standard transformation properties. For this purpose, a constant base flow is considered, to which small rotational perturbations are applied.

For the simplified two-dimensional incompressible case, the reflection positivity of the theory is shown in Section 3, which is a precondition for Wick rotation and treatment as a unitary scattering theory. The quantization is done in a natural way by identifying the particles of the theory with the molecules of the fluid. The influence of the velocity gradient in the boundary layer is assessed as an effective mass.

With this, a first order scattering theory is developed in Section 4 and a model of the origin of TS waves based on the statistical distribution of scattering events is presented in Section 5. As an approximation, only those events with the largest momentum transfer are considered. A summary and a conclusion are provided in Section 6.

1.2 Notation

In the following, vectors and higher order tensors are written in bold, \mathbf{I} and $\mathbf{0}$ denote the respective unit and zero matrix. Covariant transforming coordinates are indicated by subscripts, contravariant transforming coordinates by superscripts. Latin indices in the middle or at the end of the alphabet run from 1 to 3. For the two-dimensional Euclidean case, Latin indices in the early alphabet are used, running from 1 to 2. In Minkowski space, Greek indices are used with values ranging from 0 to 1. Einstein summation convention is used for unambiguous cases.

2 General mathematical transformations

In this section, two goals are to be achieved. First, the equation derived in Part I is transformed into a common form for gauge field theories in order to permit the subsequent application of the established concepts for quantization. In particular, the focus lies on obtaining fields with favorable transformation properties. Second, the equation is arranged in a way that the velocity field satisfies the construction conditions for the velocity gradient from Part I (Eq. 16) in a convenient way.

The starting point is the derivation of the diagonalized strain-rate tensor. It has been diagonalized by rotational and phase fields (Eq. 23 in Part I):

$$\text{tr} [\dot{\boldsymbol{\epsilon}}_{\text{diag}}] = \text{tr} [\mathbf{R}^T \dot{\boldsymbol{\epsilon}} \mathbf{R}] = \text{tr} \left[\left(\mathbf{R}^T \boldsymbol{\nabla} \right) \left(\mathbf{v}^T \mathbf{R} \mathbf{P}_{\text{diag}}^\dagger \right) \right]. \quad (1)$$

The rotational fields \mathbf{R} and the phase field $\mathbf{P}_{\text{diag}}^\dagger$ are considered directly as local fields according to the derivation in Part I. In the form Eq. 1, it becomes clear that the overall expression $\dot{\boldsymbol{\epsilon}}_{\text{diag}}$ has diagonal shape, but the inner tensor $\dot{\boldsymbol{\epsilon}}$ can be entered in any form. This degree of freedom is used to choose $\dot{\boldsymbol{\epsilon}}$ such that this tensor acquires favorable properties for inputting the initial velocity field.

The proposed transformations are performed in paragraphs 2.1 to 2.2 for this expression and inserted at the end of each paragraph into the local gauge field Eq. 71 from Part I.

2.1 Definition of projection fields

2.1.1 Location dependency/ local basis There are two perspectives to expression Eq. 1.

Perspective with respect to a global basis: According to the derivation, the local coordinate system is rotated to produce a diagonalized expression at each point. Thereby the velocity field $\mathbf{v}(\mathbf{r})$ and the gradient field $\boldsymbol{\nabla}(\mathbf{r})$ are transformed by coordinate transformations into adjusted fields $\mathbf{v}'(\mathbf{r})$ and $\boldsymbol{\nabla}'(\mathbf{r})$:

$$\begin{aligned} \text{tr} [\dot{\boldsymbol{\epsilon}}_{\text{diag}}(\mathbf{r})] &= \text{tr} \left[\left(\mathbf{R}^T(\mathbf{r}) \boldsymbol{\nabla}(\mathbf{r}) \right) \left(\mathbf{v}^T(\mathbf{r}) \mathbf{R}(\mathbf{r}) \mathbf{P}_{\text{diag}}^\dagger(\mathbf{r}) \right) \right] \\ &= \text{tr} [\boldsymbol{\nabla}'(\mathbf{r}) \mathbf{v}'^T(\mathbf{r})]. \end{aligned} \quad (2)$$

As indicated, the location dependency remains on the local fields $\mathbf{v}(\mathbf{r})$ and $\boldsymbol{\nabla}(\mathbf{r})$.

Perspective with respect to a local basis: The gradient and velocity fields are expressed with respect to an orthonormal *local* basis $\{\mathbf{f}_{\mathbf{k}}\}$. This basis can be chosen such that the first basis vector $\mathbf{f}_{\mathbf{1}}$ always points in the direction of the local velocity field $\mathbf{v}(\mathbf{r})$. In component notation, this looks as follows (using summation convention):

$$\boldsymbol{\nabla} = \mathbf{f}^k \partial_k \quad \text{and} \quad \mathbf{v}^T = \mathbf{f}_{\mathbf{n}} v^n = \mathbf{f}_{\mathbf{1}} v^1(\mathbf{r}). \quad (3)$$

In the next step, the trace is formulated as the projection of the local expression onto the global Euclidean standard basis $\{\mathbf{e}_j\}$ by means of $\text{tr } \mathbf{X} = \sum_j \mathbf{e}_j \mathbf{X} \mathbf{e}^j$. This opens a second perspective, containing the location dependency on the gauge fields. Inserting Eq. 3 into Eq. 1 yields:

$$\begin{aligned} \text{tr} [\dot{\hat{\mathbf{e}}}_{\text{diag}}(\mathbf{r})] &= \left(\mathbf{e}_j \mathbf{R}^T(\mathbf{r}) \right) \nabla \mathbf{v}^T(\mathbf{r}) \left(\mathbf{R}(\mathbf{r}) \mathbf{P}_{\text{diag}}^\dagger(\mathbf{r}) \mathbf{e}^j \right) \\ &= \left(\mathbf{e}_j \mathbf{R}^T(\mathbf{r}) \right) \mathbf{f}^k \partial_k \mathbf{f}_1 v'^1(\mathbf{r}) \left(\mathbf{R}(\mathbf{r}) \mathbf{P}_{\text{diag}}^\dagger(\mathbf{r}) \mathbf{e}^j \right) \\ &= \mathbf{O}'^T(\mathbf{r}) \mathbf{f}_1 \mathbf{f}^k \partial_k \left(v'^1(\mathbf{r}) \mathbf{O}^j(\mathbf{r}) \right). \end{aligned} \quad (4)$$

In this perspective, the rotation and phase fields form a left and a right projection field \mathbf{O}^j and \mathbf{O}'^T from the local basis $\{\mathbf{f}_k\}$ – with respect to which ∇ and \mathbf{v}^T are expressed – to the global basis $\{\mathbf{e}_j\}$. The projection fields defined in the last step of Eq. 4 are different on the right and left side:

$$\mathbf{O}^j(\mathbf{r}) = \mathbf{f}_1 \mathbf{R}(\mathbf{r}) \mathbf{P}_{\text{diag}}^\dagger(\mathbf{r}) \mathbf{e}^j \quad \text{and} \quad \mathbf{O}'^T(\mathbf{r}) = \mathbf{e}_j \mathbf{R}^T(\mathbf{r}) \mathbf{f}^1. \quad (5)$$

With this interpretation, the direction dependency passes from the local quantities ∂_k and v'^m to the projection fields Eq. 5, which contain the coordinate transformation from the local basis to the global basis. $v'^1(\mathbf{r})$ includes only the information on the location-dependent velocity magnitude, not on the direction. The local basis vector \mathbf{f}_1 is included in the projection function for later convenience.

Remark 1 *Using this perspective, the local basis $\{\mathbf{f}_k\}$, with respect to which the fields ∇ and \mathbf{v} are expressed, can be chosen freely. This is possible because a change of the local basis will be incorporated by the projection fields such that the total expression remains diagonal. This has been utilized directly in the definition of the basis system $\{\mathbf{f}_k\}$ in Eq. 3.*

Eq. 4 inserted into Eq. 71 from Part I using Eq. 73 from Part I results in the overall stress tensor:

$$\begin{aligned} \rho^{-1} \text{tr} [\boldsymbol{\sigma}_{\text{local}}(\mathbf{r})] &= \left(\frac{\zeta^{SI}}{\mu^{SI}} + \frac{4}{3} \right) Re_C^{-1} \mathbf{O}'^T(\mathbf{r}) \mathbf{f}_1 \mathbf{f}^k D_k \left(v'^1(\mathbf{r}) \mathbf{O}^j(\mathbf{r}) \right) \\ &\quad + \frac{1}{4} \mathbf{G}'^m{}_{jk} \mathbf{G}'^m{}^{jk} + \frac{1}{4} \mathbf{F}'_{jk} \mathbf{F}'^{jk}. \end{aligned} \quad (6)$$

with (according to Eq. 72 from Part I):

$$\mathbf{D} = \nabla - ig \mathbf{A}'_{\perp}{}^m - ig' \mathbf{A}'_{\parallel}. \quad (7)$$

2.1.2 Splitting the phase field For the spatial derivative of scalar functions $x(\mathbf{r})$, it is generally true that:

$$\nabla x^2 = 2x \nabla x, \quad (8)$$

which can be used to split the phase $\mathbf{P}_{\text{diag}}^\dagger(\mathbf{r}) = \mathbf{I}e^{i\theta(\mathbf{r})}$ symmetrically on both projection fields. This motivates the definition of an adjusted projection field $\mathbf{Q}^j(\mathbf{r})$ with respect to Eq. 5:

$$\mathbf{Q}^j(\mathbf{r}) = \mathbf{f}_1 \mathbf{R}(\mathbf{r}) e^{i\theta(\mathbf{r})/2} \mathbf{e}^j \quad \text{and} \quad \mathbf{Q}_j^T(\mathbf{r}) = \mathbf{e}_j e^{i\theta(\mathbf{r})/2} \mathbf{R}^T(\mathbf{r}) \mathbf{f}^1, \quad (9)$$

with the help of which the strain-rate tensor Eq. 4 can be expressed as a function of the field $\mathbf{Q}^j(\mathbf{r})$ and its transpose $\mathbf{Q}_j^T(\mathbf{r})$:

$$\text{tr} [\dot{\boldsymbol{\epsilon}}_{\text{diag}}(\mathbf{r})] = \mathbf{Q}_j^T(\mathbf{r}) \mathbf{f}_1 \mathbf{f}^k \partial_k (v^1(\mathbf{r}) \mathbf{Q}^j(\mathbf{r})). \quad (10)$$

When inserting into stress tensor Eq. 6, the coupling must be adapted to the redefined phase field:

$$\begin{aligned} \rho^{-1} \text{tr} [\boldsymbol{\sigma}_{\text{local}}(\mathbf{r})] &= \left(\frac{\zeta^{SI}}{\mu^{SI}} + \frac{4}{3} \right) Re_C^{-1} \mathbf{Q}_j^T(\mathbf{r}) \mathbf{f}_1 \mathbf{f}^k D'_k (v^1(\mathbf{r}) \mathbf{Q}^j(\mathbf{r})) \\ &\quad + \frac{1}{4} \mathbf{G}'^m{}_{jk} \mathbf{G}'^m{}_{jk} + \frac{1}{4} \mathbf{F}'_{jk} \mathbf{F}'^{jk}, \end{aligned} \quad (11)$$

with

$$\mathbf{D}' = \nabla - ig \mathbf{A}'_{\perp}{}^m - 2ig' \mathbf{A}'_{\parallel}. \quad (12)$$

Where the covariant derivative \mathbf{D}' has been adjusted compared to Eq. 7 so that the doubled coupling constant compensates for the halved field strength of the right phase field on which the derivative is acting.

2.2 Adjoint projection fields

Except for the phase field $e^{i\theta(\mathbf{r})/2}$, the two projection fields \mathbf{Q}^j and \mathbf{Q}_j^T (Eq. 9) form the conjugate transpose (adjoint) to each other. However, the phase field destroys the adjointness. This leaves Eq. 11 invariant under orthogonal transformations but not under unitary transformations, which complicates the analytic continuation.

In this section, a consistent treatment for the phase field is proposed, using a description with adjoint projection fields. The procedure is based initially on an extension of the underlying equation by introducing an additional symmetry plane. When restricting to the two-dimensional case in Section 3, the extended system can be separated again, thus introducing the adjoint fields without increasing complexity.

2.2.1 Separating shear and vorticity parts by projection into the Clifford algebra For further argumentation, an explicit local basis $\{\mathbf{f}^{\mathbf{k}}\}$ is introduced. According to the construction, the symmetric shear part of the flow has to be inserted into the velocity gradient as real and the skew-symmetric vorticity part as imaginary values (Eq. 16 in Part I). Thus, it is beneficial to choose a basis in which real and imaginary coordinates are separated automatically into symmetric and skew-symmetric parts of the flow.

The subalgebra $\Lambda^2(\mathbb{R}^3)$ of the outer algebra $\Lambda(\mathbb{R}^3)$ forms a basis of the skew-symmetric matrices. This motivates to project the local basis vectors $\{\mathbf{f}^{\mathbf{k}}\}$ into the outer algebra where they first span the subalgebra of vectorially transforming elements $\mathbb{R}^3 \rightarrow \Lambda^1(\mathbb{R}^3)$ (Renaud, 2022). The dyadic product $\mathbf{f}^{\mathbf{k}}\mathbf{f}_{\mathbf{j}}$ in Eq. 10 subsequently forms a basis of the desired subalgebra of skew-symmetric matrices $\Lambda^2(\mathbb{R}^3)$ plus the unit matrix \mathbf{I} .

On the other hand, the outer algebra on Euclidean space is equal to the Clifford algebra, determining the specific form of the basis: In three dimensions the corresponding Clifford algebra is given by $\Lambda(\mathbb{R}^3) = Cl(3,0)_{\mathbb{R}}$ (which is extended by analytic continuation to $Cl(3)_{\mathbb{C}}$), with the defining anticommutative property:

$$\{\mathbf{f}^{\mathbf{j}}, \mathbf{f}^{\mathbf{k}}\} = \mathbf{f}^{\mathbf{j}}\mathbf{f}^{\mathbf{k}} + \mathbf{f}^{\mathbf{k}}\mathbf{f}^{\mathbf{j}} = 2\delta^{jk}\mathbf{I}. \quad (13)$$

Thus, a possible projection of the local basis vectors $\mathbb{R}^3 \rightarrow Cl(3,0)_{\mathbb{R}}$ is specified by the Pauli matrices:

$$\mathbf{f}^{\mathbf{1}} = \boldsymbol{\sigma}^1 = \begin{pmatrix} 0 & 1 \\ 1 & 0 \end{pmatrix} \quad \mathbf{f}^{\mathbf{2}} = \boldsymbol{\sigma}^2 = \begin{pmatrix} 0 & -i \\ i & 0 \end{pmatrix} \quad \mathbf{f}^{\mathbf{3}} = \boldsymbol{\sigma}^3 = \begin{pmatrix} 1 & 0 \\ 0 & -1 \end{pmatrix}. \quad (14)$$

With this, the dyadic products $\{\mathbf{f}^{\mathbf{k}}\mathbf{f}_{\mathbf{j}}\}$ for $j \neq k$, using the $\mathbf{f}^{\mathbf{k}}$ according to Eq. 14, form a generating set of a space isomorphic to the skew-symmetric matrices over the \mathbb{R}^3 .

Simultaneously, these generators multiplied by i , namely $\{i\mathbf{f}^{\mathbf{k}}\mathbf{f}_{\mathbf{j}}\}$ for $j \neq k$ as well as $\mathbf{f}^{\mathbf{1}}\mathbf{f}_{\mathbf{1}} = \mathbf{I}$ generate a space isomorphic to a part of the symmetric matrices over the \mathbb{R}^3 . More precisely, they span a four-dimensional subspace of the six-dimensional space of symmetric matrices over \mathbb{R}^3 . Since we are ultimately interested in the three-dimensional space of diagonal symmetric matrices, the dimensionality of $\{i\mathbf{f}^{\mathbf{k}}\mathbf{f}_{\mathbf{j}}\}$ is sufficient to introduce any meaningful initial conditions in a practical way. The remaining symmetric matrices can be obtained by similarity transformations.

Therefore, in this basis the symmetrical and skew-symmetrical parts of the velocity gradient are directly partitioned into real and imaginary parts of the coordinates. However, they are still partially interchanged. Therefore the velocity field is redefined to:

$$v^1(\mathbf{r}) = iv^1(\mathbf{r}), \quad (15)$$

yielding when inserted into the strain-rate tensor Eq. 10:

$$\text{tr}[\dot{\boldsymbol{\epsilon}}_{\text{diag}}(\mathbf{r})] = \mathbf{Q}_{\mathbf{j}}^{\text{T}}(\mathbf{r})\mathbf{f}_{\mathbf{1}}\mathbf{f}^{\mathbf{k}}\partial_k(iv^1(\mathbf{r})\mathbf{Q}^{\mathbf{j}}(\mathbf{r})). \quad (16)$$

In this representation, the initial velocity field v^1 can be introduced straightforwardly as a scalar field whose gradient corresponds to the local shear and vorticity strengths ω^{shear} and $\omega^{\text{vorticity}}$. In components this reads:

$$\partial_k v^1(\mathbf{r}) = \omega_k^{\text{shear}} + i\omega_k^{\text{vorticity}}. \quad (17)$$

Please note that in flow direction x^1 the roles of shear and vorticity are reversed initially. However, this reversal is later eliminated by the Wick rotation $x^1 \rightarrow ix^1$, which is required independently for the formulation of the scattering theory.

Thus, the choice of basis Eq. 14 ensures that the real parts enter the equation in hermitian and the complex parts in skew-hermitian form (isomorphic to symmetric and skew-symmetric parts over the \mathbb{R}^3) and is used in the following.

Remark 2 *The space spanned by the Pauli matrices $\mathbf{x} = \mathbf{f}^k x_k$, $x_k \in \mathbb{R}$ together with the scalar product $\langle \mathbf{xy} \rangle = \frac{1}{2} \text{tr}(\mathbf{xy})$ continues to form a representation of Euclidean space. The Pauli matrices $\{\mathbf{f}^j\} = \{\boldsymbol{\sigma}^j\}$ are in this case to be understood as a projection of the canonical basis of Euclidean space into the Clifford algebra. More precisely, they span the subspace $Cl^1(3,0) = \mathbb{R}^3$ of the vectorial transforming elements of $Cl(3,0)$, resp. their analytic extension (Renaud, 2022).*

The algebra of rotations can be expressed in terms of this basis as:

$$\mathbf{L}^{\mathbf{m}} = -\frac{i}{4} [\mathbf{f}^{\mathbf{n}}, \mathbf{f}^{\mathbf{l}}] = -\frac{i}{4} (\mathbf{f}^{\mathbf{n}} \mathbf{f}^{\mathbf{l}} - \mathbf{f}^{\mathbf{l}} \mathbf{f}^{\mathbf{n}}) = \frac{1}{2} \epsilon^{mnl} \boldsymbol{\sigma}^{\mathbf{m}}, \quad (18)$$

with the transformations:

$$\mathbf{R} = e^{\frac{i}{2} \phi_m \boldsymbol{\sigma}^{\mathbf{m}}} \approx \mathbf{I} + \frac{i}{2} \phi_m \boldsymbol{\sigma}^{\mathbf{m}}. \quad (19)$$

and the transformation rule for vectors \mathbf{w} (e.g. Straub, 2016):

$$\mathbf{w}' = \mathbf{R} \mathbf{w} \mathbf{R}^\dagger. \quad (20)$$

Because the rotation fields in this description are not purely real anymore, in this basis Eq. 16 must be adjusted:

$$\text{tr} [\dot{\boldsymbol{\epsilon}}_{\text{diag}}(\mathbf{r})] = \mathbf{e}_j e^{i\theta(\mathbf{r})/2} \mathbf{R}^\dagger(\mathbf{r}) \mathbf{f}_1 \mathbf{f}^1 \mathbf{f}^k \partial_k (i v_1(\mathbf{r}) \mathbf{Q}^j(\mathbf{r})), \quad (21)$$

since the left side can no longer be expressed as $\mathbf{Q}_j^{\mathbf{T}}$. In addition, it is used that in the chosen basis (Eq. 14) it holds that $\mathbf{f}^1 = \mathbf{f}_1 = (\mathbf{f}_1)^* = (\mathbf{f}_1)^{\mathbf{T}}$.

Remark 3 *The transition to the description of the rotation fields as $SU(2)$ -fields is a purely computational step exploiting the isomorphism between the Lie algebras $su(2) \cong so(3)$ which allows to formulate the scattering theory according to standard literature. The physical rotations continue to transform as $SO(3)$ fields and would need to be back-transformed if needed. With respect to the Clifford algebra, they span the subspace $Cl^2(3,0)$ of the bivectorially transforming elements of $Cl(3,0)$.*

2.2.2 Auxiliary tensor with complex conjugated phase As noted in Par. 2.4.2 in Part I, the phase $e^{i\theta}$ is not a global symmetry of the strain-rate tensor $\dot{\boldsymbol{\varepsilon}}$, but only of the tensor $\dot{\boldsymbol{\varepsilon}}^*\dot{\boldsymbol{\varepsilon}}$. For the perturbative calculation it is sufficient to consider small phases ($e^{i\theta} \approx 1 + i\theta$), which makes it possible to generate a phase-invariant expression by adding to the existing trace a complex conjugate strain-rate tensor $\dot{\boldsymbol{\varepsilon}}^*$ with inverted phase:

$$\text{tr}[\tilde{\boldsymbol{\varepsilon}}] = \frac{1}{2}\text{tr}[\dot{\boldsymbol{\varepsilon}}] + \frac{1}{2}\text{tr}[\dot{\boldsymbol{\varepsilon}}^*]. \quad (22)$$

Since the original strain-rate tensor is real-valued in its unperturbed form, this expression remains invariant in first order under phase transformations:

$$\begin{aligned} \text{tr}[\tilde{\boldsymbol{\varepsilon}}] &= \frac{1}{2}\text{tr}[\dot{\boldsymbol{\varepsilon}}e^{i\theta}] + \frac{1}{2}\text{tr}[\dot{\boldsymbol{\varepsilon}}^*e^{-i\theta}] \\ &\approx \frac{1}{2}\text{tr}[\dot{\boldsymbol{\varepsilon}}(1 + i\theta)] + \frac{1}{2}\text{tr}[\dot{\boldsymbol{\varepsilon}}^*(1 - i\theta)] \\ &= \frac{1}{2}\text{tr}[\dot{\boldsymbol{\varepsilon}}] + \frac{1}{2}\text{tr}[\dot{\boldsymbol{\varepsilon}}^*] + O(\theta^2). \end{aligned} \quad (23)$$

The extended phase-invariant strain-rate tensor $\tilde{\boldsymbol{\varepsilon}}$ is denoted with a tilde below the symbol. The complex conjugation can be performed at first on the original, non-diagonalized strain-rate tensor:

$$\begin{aligned} \dot{\boldsymbol{\varepsilon}}^*(\mathbf{r}) &= \left(e^{i\theta(\mathbf{r})/2} \mathbf{f}^1 \mathbf{f}^k \partial_k (i v_1(\mathbf{r}) e^{i\theta(\mathbf{r})/2}) \right)^* \\ &= e^{-i\theta(\mathbf{r})/2} \mathbf{f}^1 (\mathbf{f}^k)^* \partial_k (-i v_1^*(\mathbf{r}) e^{-i\theta(\mathbf{r})/2}). \end{aligned} \quad (24)$$

The complex conjugate tensor in Eq. 24 can be transformed some further using similarity transformations, allowing the definition of adjoint projection fields. The trace $\text{tr}[\dot{\boldsymbol{\varepsilon}}^*]$ of the tensor does not change in consequence. First, the same similarity transformation is applied to the complex conjugate tensor $\dot{\boldsymbol{\varepsilon}}^*$ as to the original tensor (Eq. 21), yielding the tensor $\dot{\boldsymbol{\varepsilon}}'$:

$$\begin{aligned} \text{tr}[\dot{\boldsymbol{\varepsilon}}'(\mathbf{r})] &= \text{tr}[\mathbf{R}^\dagger(\mathbf{r}) \dot{\boldsymbol{\varepsilon}}^*(\mathbf{r}) \mathbf{R}(\mathbf{r})] \\ &= \mathbf{e}_j e^{-i\theta(\mathbf{r})/2} \mathbf{R}^\dagger(\mathbf{r}) \mathbf{f}_1 \mathbf{f}^1 (\mathbf{f}^k)^* \partial_k (-i v_1^*(\mathbf{r}) \mathbf{f}^1 \mathbf{R}(\mathbf{r}) e^{-i\theta(\mathbf{r})/2} \mathbf{e}^j). \end{aligned} \quad (25)$$

In addition, for further use, the tensor is rotated by π in the real plane. The mirrored and rotated tensor $\hat{\boldsymbol{\varepsilon}}$ is marked with a breve below the symbol:

$$\begin{aligned} \text{tr}[\hat{\boldsymbol{\varepsilon}}(\mathbf{r})] &= \text{tr}[-i \boldsymbol{\sigma}_2^\dagger \dot{\boldsymbol{\varepsilon}}'(\mathbf{r}) i \boldsymbol{\sigma}^2] \\ &= \mathbf{e}_j \boldsymbol{\sigma}_2^\dagger e^{-i\theta(\mathbf{r})/2} \mathbf{R}^\dagger(\mathbf{r}) \mathbf{f}_1 \mathbf{f}^1 (\mathbf{f}^k)^* \partial_k (-i v_1^*(\mathbf{r}) \mathbf{f}^1 \mathbf{R}(\mathbf{r}) e^{-i\theta(\mathbf{r})/2} \boldsymbol{\sigma}^2 \mathbf{e}^j) \\ &= \mathbf{e}_j e^{-i\theta(\mathbf{r})/2} \mathbf{R}^\mathbf{T}(\mathbf{r}) \mathbf{f}_1 \mathbf{f}^1 \mathbf{f}^k \partial_k (-i v_1^*(\mathbf{r}) \mathbf{f}^1 \mathbf{R}^*(\mathbf{r}) e^{-i\theta(\mathbf{r})/2} \boldsymbol{\sigma}_2^\dagger \boldsymbol{\sigma}^2 \mathbf{e}^j) \\ &= \mathbf{e}_j e^{-i\theta(\mathbf{r})/2} \mathbf{R}^\mathbf{T}(\mathbf{r}) \mathbf{f}_1 \mathbf{f}^1 \mathbf{f}^k \partial_k (-i v_1^*(\mathbf{r}) \mathbf{f}^1 \mathbf{R}^*(\mathbf{r}) e^{-i\theta(\mathbf{r})/2} \mathbf{e}^j) \\ &= \mathbf{e}_j e^{-i\theta(\mathbf{r})/2} \mathbf{R}^\mathbf{T}(\mathbf{r}) \mathbf{f}_1 \mathbf{f}^1 \mathbf{f}^k \partial_k (-i v_1^*(\mathbf{r}) \mathbf{Q}^{*j}(\mathbf{r})). \end{aligned} \quad (26)$$

In this calculation, the following permutation property of σ^2 with all Pauli matrices σ^m was applied:

$$-\sigma^2 \sigma^{*m} = +\sigma^m \sigma^2, \quad (27)$$

and consequently for the rotations:

$$\sigma^2 \mathbf{R}^* \approx \sigma^2 \left(\mathbf{I} - \frac{i}{2} \phi_m \sigma^{*m} \right) = \left(\mathbf{I} + \frac{i}{2} \phi_m \sigma^m \right) \sigma^2 \approx \mathbf{R} \sigma^2. \quad (28)$$

Tensor Eq. 26 is used to form the extended, semi-diagonalized strain-rate tensor $\dot{\hat{\epsilon}}_{\text{hdiag}}$, whose trace is given by:

$$\text{tr}[\dot{\hat{\epsilon}}_{\text{hdiag}}(\mathbf{r})] = \frac{1}{2} \text{tr}[\dot{\hat{\epsilon}}_{\text{diag}}(\mathbf{r})] + \frac{1}{2} \text{tr}[\dot{\hat{\epsilon}}(\mathbf{r})], \quad (29)$$

with partial tensors according to Eqs. 21 and 26 and invariant in first order under phase transformations as shown in Eq. 23. This configuration can be used to define adjoint projection fields.

Remark 4 *Please note that the complex conjugate auxiliary tensor $\hat{\epsilon}$ does in general not have diagonal shape in the three-dimensional case. However, in the two-dimensional case (from Section 3 onwards), both tensors $\dot{\hat{\epsilon}}$ and $\hat{\epsilon}$ are diagonalized simultaneously. Diagonal shape is not a necessary condition for the introduction of adjoint projection fields in this section.*

2.2.3 Doubled strain-rate tensor and adjoint phase To construct Eqs. 21 and 26 by means of adjoint projection fields with respect to \mathbf{Q}^j , the eigenvalues of the squared strain-rate tensor are considered first. For a unitary matrix \mathbf{C} it holds that:

$$\dot{\hat{\epsilon}}_{\text{diag}}^\dagger \dot{\hat{\epsilon}}_{\text{diag}} = \dot{\hat{\epsilon}}_{\text{diag}}^\dagger \mathbf{C}^\dagger \mathbf{C} \dot{\hat{\epsilon}}_{\text{diag}} = (\dot{\hat{\epsilon}}_{\text{diag}}^{\mathbf{C}})^\dagger \dot{\hat{\epsilon}}_{\text{diag}}^{\mathbf{C}}. \quad (30)$$

And analogously for the mirrored strain-rate tensor $\hat{\epsilon}$. \mathbf{C} is chosen to be:

$$\mathbf{C} = \sigma^2, \quad (31)$$

with which the trace of the slightly adjusted tensor $\dot{\hat{\epsilon}}_{\text{diag}}^{\mathbf{C}}$, defined in the last step of Eq. 30, can be written as (starting from Eq. 21, the projection fields as defined by Eq. 9, and subsequent application of permutation relations Eqs. 27 and 28):

$$\begin{aligned} \text{tr}[\dot{\hat{\epsilon}}_{\text{diag}}^{\mathbf{C}}(\mathbf{r})] &= \text{tr}[\mathbf{C} \dot{\hat{\epsilon}}_{\text{diag}}(\mathbf{r})] \\ &= \mathbf{e}_j \mathbf{C} e^{i\theta(\mathbf{r})/2} \mathbf{R}^\dagger(\mathbf{r}) \mathbf{f}_1 \mathbf{f}^1 \mathbf{f}^k \partial_k (iv_1(\mathbf{r}) \mathbf{Q}^j(\mathbf{r})) \\ &= \mathbf{e}_j e^{i\theta(\mathbf{r})/2} \mathbf{R}^T(\mathbf{r}) \mathbf{f}_1 \mathbf{f}^1 \mathbf{C} \mathbf{f}^k \partial_k (iv_1(\mathbf{r}) \mathbf{Q}^j(\mathbf{r})) \\ &= \mathbf{Q}_j^T(\mathbf{r}) \mathbf{f}^1 \mathbf{C} \mathbf{f}^k \partial_k (iv_1(\mathbf{r}) \mathbf{Q}^j(\mathbf{r})), \end{aligned} \quad (32)$$

as well as for the mirrored tensor $\hat{\epsilon}^{\mathbf{C}}$ (starting from Eq. 26):

$$\begin{aligned}
\text{tr}[\dot{\underline{\hat{\epsilon}}}^{\text{C}}(\mathbf{r})] &= \text{tr}[\mathbf{C}^* \dot{\underline{\hat{\epsilon}}}(\mathbf{r})] \\
&= \mathbf{e}_j \mathbf{C}^* e^{-i\theta(\mathbf{r})/2} \mathbf{R}^{\text{T}}(\mathbf{r}) \mathbf{f}_1 \mathbf{f}^1 \mathbf{f}^k \partial_k (-iv_1^*(\mathbf{r}) \mathbf{Q}^{*j}(\mathbf{r})) \\
&= \mathbf{e}_j e^{-i\theta(\mathbf{r})/2} \mathbf{R}^\dagger(\mathbf{r}) \mathbf{f}_1 \mathbf{f}^1 \mathbf{C}^* \mathbf{f}^k \partial_k (-iv_1^*(\mathbf{r}) \mathbf{Q}^{*j}(\mathbf{r})) \\
&= \mathbf{Q}_j^\dagger(\mathbf{r}) \mathbf{f}^1 \mathbf{C}^* \mathbf{f}^k \partial_k (-iv_1^*(\mathbf{r}) \mathbf{Q}^{*j}(\mathbf{r})).
\end{aligned} \tag{33}$$

The combined trace of these two tensors $\text{tr}[\dot{\underline{\hat{\epsilon}}}_{\text{hdiag}}^{\text{C}}] = \frac{1}{2} \text{tr}[\dot{\underline{\hat{\epsilon}}}_{\text{diag}}^{\text{C}}] + \frac{1}{2} \text{tr}[\dot{\underline{\hat{\epsilon}}}^{\text{C}}]$ can be written with adjoint projection fields. For this purpose, a ‘‘doubled’’ projection field $\underline{\mathbf{Q}}^j$ is considered by inserting the complex conjugate field \mathbf{Q}^{*j} below the original projection field from Eq. 9:

$$\underline{\mathbf{Q}}^j(\mathbf{r}) = \begin{pmatrix} \mathbf{Q}^j(\mathbf{r}) \\ \mathbf{Q}^{*j}(\mathbf{r}) \end{pmatrix} = \begin{pmatrix} \mathbf{f}^1 \mathbf{R}(\mathbf{r}) e^{i\theta(\mathbf{r})/2} \mathbf{e}^j \\ \mathbf{f}^1 \mathbf{R}^*(\mathbf{r}) e^{-i\theta(\mathbf{r})/2} \mathbf{e}^j \end{pmatrix}. \tag{34}$$

Together with a permutation matrix:

$$\underline{\mathbf{C}} = \begin{pmatrix} \mathbf{0} & \mathbf{C}^* \\ \mathbf{C} & \mathbf{0} \end{pmatrix} = \begin{pmatrix} \mathbf{0} & -\sigma^2 \\ \sigma^2 & \mathbf{0} \end{pmatrix}, \tag{35}$$

and the shorthand notation:

$$\underline{\mathbf{f}}^1 \underline{\mathbf{f}}^k \underline{\partial}_k i v_1(\mathbf{r}) = \begin{pmatrix} \mathbf{f}^1 \mathbf{f}^k \partial_k i v_1(\mathbf{r}) & 0 \\ 0 & -\mathbf{f}^1 \mathbf{f}^k \partial_k i v_1^*(\mathbf{r}) \end{pmatrix}, \tag{36}$$

the combined trace can be expressed as follows:

$$\begin{aligned}
\text{tr}[\dot{\underline{\hat{\epsilon}}}_{\text{hdiag}}^{\text{C}}(\mathbf{r})] &= \frac{1}{2} \left(\mathbf{Q}_j^\dagger(\mathbf{r}) \underline{\mathbf{f}}^1 \underline{\mathbf{C}} \underline{\mathbf{f}}^k \underline{\partial}_k \right) \left(i v_1(\mathbf{r}) \underline{\mathbf{Q}}^j(\mathbf{r}) \right) \\
&= \frac{1}{2} \left(\mathbf{Q}_j^\text{T}(\mathbf{r}) \mathbf{f}^1 \mathbf{C} \mathbf{f}^k \partial_k \right) \left(i v_1(\mathbf{r}) \mathbf{Q}^j(\mathbf{r}) \right) \\
&\quad + \frac{1}{2} \left(\mathbf{Q}_j^\dagger(\mathbf{r}) \mathbf{f}^1 \mathbf{C}^* \mathbf{f}^k \partial_k \right) \left(-i v_1^*(\mathbf{r}) \mathbf{Q}^{*j}(\mathbf{r}) \right) \\
&= \frac{1}{2} \text{tr}[\dot{\underline{\hat{\epsilon}}}_{\text{diag}}^{\text{C}}(\mathbf{r})] + \frac{1}{2} \text{tr}[\dot{\underline{\hat{\epsilon}}}^{\text{C}}(\mathbf{r})].
\end{aligned} \tag{37}$$

With this, a form is found in which the projection fields $\underline{\mathbf{Q}}_j^\dagger$ and $\underline{\mathbf{Q}}^j$ (Eq. 34) form adjoint fields to each other. As a last step, the following shorthand notation for the left projection field is introduced:

$$\overline{\mathbf{Q}}_j(\mathbf{r}) = \mathbf{Q}_j^\dagger(\mathbf{r}) i \underline{\mathbf{f}}^1 \underline{\mathbf{C}}. \tag{38}$$

This yields, substituted into Eq. 37, for the doubled strain-rate tensor:

$$\text{tr}[\dot{\underline{\hat{\epsilon}}}_{\text{hdiag}}^{\text{C}}(\mathbf{r})] = \frac{1}{2} \overline{\mathbf{Q}}_j(\mathbf{r}) \underline{\mathbf{f}}^k \underline{\partial}_k (v_1(\mathbf{r}) \underline{\mathbf{Q}}^j(\mathbf{r})). \tag{39}$$

Remark 5 $\dot{\epsilon}_{\text{diag}}^{\text{C}}$ does no longer correspond exactly to the original strain-rate tensor due to the additional matrix \mathbf{C} according to Eq. 16. However, by constructing it through Eq. 30, it is guaranteed that the eigenvalues squared are the same. The eigenvalues of $\dot{\epsilon}_{\text{diag}}^{\text{C}}$ thus coincide with the eigenvalues of the original strain-rate tensor $\dot{\epsilon}_{\text{diag}}$ except for a global phase. The connection between the solutions for $\dot{\epsilon}_{\text{diag}}$ and $\dot{\epsilon}_{\text{diag}}^{\text{C}}$ is discussed in Section 6.2.

2.2.4 Insertion into the stress tensor and field connection To express the doubled stress tensor associated with the doubled strain-rate tensor Eq. 39, the behavior of the coupling upon reflection must be taken into account. For the doubled covariant derivative together with the complex conjugation this results in:

$$\mathbf{D}' = \begin{pmatrix} \mathbf{D}' & \mathbf{0} \\ \mathbf{0} & \mathbf{D}' \end{pmatrix}, \quad (40)$$

with (from Eq. 12):

$$\begin{aligned} \mathbf{D}' &= \nabla - ig\mathbf{A}'_{\perp}{}^m - 2ig'\mathbf{A}'_{\parallel} \\ \mathbf{D}' &= \nabla + ig(\mathbf{A}'_{\perp}{}^m)^* + 2ig'\mathbf{A}'_{\parallel}. \end{aligned} \quad (41)$$

The adjoint fields and the doubled strain-rate tensor are transferred into Eq. 11 and one obtains for the doubled stress tensor:

$$\begin{aligned} \rho^{-1} \text{tr} [\boldsymbol{\sigma}'_{\text{local}}(\mathbf{r})] &= \frac{1}{2} \left(\frac{\zeta^{SI}}{\mu^{SI}} + \frac{4}{3} \right) Re_c^{-1} \bar{\mathbf{Q}}_j(\mathbf{r}) \mathbf{f}^k D'_k (v_1(\mathbf{r}) \mathbf{Q}^j(\mathbf{r})) \\ &+ \frac{1}{8} \mathbf{G}'^m{}_{jk} \mathbf{G}'^m{}_{jk} + \frac{1}{8} \mathbf{G}'^m{}_{jk} \mathbf{G}'^m{}_{jk} + \frac{1}{4} \mathbf{F}'_{jk} \mathbf{F}'^{jk}, \end{aligned} \quad (42)$$

with the complex conjugated rotational fields:

$$\mathbf{G}'^m{}_{jk} = \left(\mathbf{G}'^m{}_{jk} \right)^*. \quad (43)$$

3 Problem specific simplifications and adjustments

In this section, the field equation is maximally simplified to formulate the most elementary scattering theory. For this purpose, the boundary layer flow over the flat plate (Fig. 1) is represented as a two-dimensional, incompressible flow in x_1 -direction and, in addition, the gradient of the velocity field normal to the flow direction is linearly approximated.

In this framework, the remaining properties for the formulation of a scattering theory – such as normalization and reflection positivity – are established, before Wick rotation and quantization take place.

Nomenclature is adapted according to the two-dimensionality: Latin indices a, b run from 1 to 2 and after Wick rotation Greek indices α, β run from 0 to 1.

3.1 Incompressible two-dimensional flow

In the example, an incompressible flow is considered. Thus, the density remains constant $\rho = \frac{\rho^{SI}}{\rho_\infty^{SI}} = 1$ and the volume viscosity can be neglected $\zeta^{SI} \approx 0$, whereby also the coupling to the phase field $g \approx 0$ vanishes (Eq. 74 in Part I).

Due to the two-dimensionality, for the Clifford algebra $Cl^1(2, 0)$ a chiral basis can be chosen, e.g.:

$$\mathbf{f}^1 = \boldsymbol{\sigma}^1 = \begin{pmatrix} 0 & 1 \\ 1 & 0 \end{pmatrix} \quad \mathbf{f}^2 = \boldsymbol{\sigma}^2 = \begin{pmatrix} 0 & -i \\ i & 0 \end{pmatrix}. \quad (44)$$

With respect to the chiral basis Eq. 44, the rotations take diagonal form, the only generator is:

$$\mathbf{L}^3 = -\frac{i}{4} [\mathbf{f}^1, \mathbf{f}^2] = \frac{1}{2} \boldsymbol{\sigma}^3 \quad \text{and} \quad \mathbf{L}_\perp^3 = -\frac{1}{2} \boldsymbol{\sigma}^3 = -\mathbf{L}^3, \quad (45)$$

where $\boldsymbol{\sigma}^3 \in Cl^2(2, 0)$. The corresponding rotations are given by:

$$\mathbf{R}(\mathbf{r}) = e^{\frac{i}{2}\phi_3(\mathbf{r})\boldsymbol{\sigma}^3} \quad \text{and} \quad \mathbf{R}_\perp(\mathbf{r}) = e^{-\frac{i}{2}\phi_3(\mathbf{r})\boldsymbol{\sigma}^3} = \mathbf{R}^*(\mathbf{r}). \quad (46)$$

Thus, the two-dimensional abelian rotation potential $\mathbf{A}'_{\perp}{}^{2D}$ is formed by the third component (perpendicular to the considered plane) of the original three-dimensional potential Eq. 68 in Part I:

$$\mathbf{A}'_{\perp}{}^{2D} = \nabla\phi(\mathbf{r})\mathbf{L}^3, \quad (47)$$

The covariant derivative and the coupling to the rotational gauge field are simplified compared to Eq. 12 to:

$$\mathbf{D} = \mathbf{D}' = \nabla - ig_{2D}\mathbf{A}'_{\perp}{}^{2D} \quad g_{2D} = \frac{3}{2\sqrt{2}}\sqrt{Re_C}. \quad (48)$$

For the doubled covariant derivative, it holds that (compare to Eq. 41):

$$\underline{\mathbf{D}} = \begin{pmatrix} \mathbf{D} & \mathbf{0} \\ \mathbf{0} & \mathbf{D}_\perp \end{pmatrix} = \begin{pmatrix} \nabla - ig_{2D}\mathbf{A}'_{\perp}{}^{2D} & \mathbf{0} \\ \mathbf{0} & \nabla + ig_{2D}\mathbf{A}'_{\perp}{}^{2D} \end{pmatrix} = \begin{pmatrix} \mathbf{D} & \mathbf{0} \\ \mathbf{0} & \mathbf{D}^* \end{pmatrix}. \quad (49)$$

The chiral element $\boldsymbol{\sigma}^5$ takes diagonal form in the selected basis:

$$\boldsymbol{\sigma}^5 = i\boldsymbol{\sigma}^1\boldsymbol{\sigma}^2 = \begin{pmatrix} -1 & 0 \\ 0 & 1 \end{pmatrix}. \quad (50)$$

The upper and lower components of the two-dimensional projection fields \mathbf{Q}^a do not mix under rotations and can be split into their chiral parts. In addition, the phase can be set to zero $\theta(\mathbf{r}) = 0$, since the phase field does not couple in the incompressible

case. This results in the simplified projection fields compared to the general case (Eq. 9):

$$\mathbf{Q}^{\mathbf{a}}(\mathbf{r}) = \begin{pmatrix} Q_L^{\mathbf{a}}(\mathbf{r}) \\ Q_R^{\mathbf{a}}(\mathbf{r}) \end{pmatrix} = \mathbf{f}^{\mathbf{1}}\mathbf{R}(\mathbf{r})\mathbf{e}^{\mathbf{a}} = \mathbf{f}^{\mathbf{1}}e^{i\phi_3(\mathbf{r})\mathbf{L}^3}\mathbf{e}^{\mathbf{a}}, \quad (51)$$

and consequently for the doubled projection fields (Eq. 34):

$$\underline{\mathbf{Q}}^{\mathbf{a}}(\mathbf{r}) = \begin{pmatrix} \mathbf{Q}^{\mathbf{a}}(\mathbf{r}) \\ \mathbf{Q}^{*\mathbf{a}}(\mathbf{r}) \end{pmatrix} \quad \text{and} \quad \bar{\mathbf{Q}}_{\mathbf{a}}(\mathbf{r}) = \underline{\mathbf{Q}}_{\mathbf{a}}^{\dagger}(\mathbf{r}) i\mathbf{f}^{\mathbf{1}}\underline{\mathbf{C}}. \quad (52)$$

The $Q_{L/R}^{\mathbf{a}}$ denote the respective left- and right-handed chiral parts of the fields. As usual, these can be separated using the projection operators $\mathbf{P}_{L/R} = \frac{1}{2}(\mathbf{1} \mp \boldsymbol{\sigma}^5)$.

$\underline{\mathbf{C}}$ remains unchanged:

$$\underline{\mathbf{C}} = \begin{pmatrix} \mathbf{0} & \mathbf{C}^* \\ \mathbf{C} & \mathbf{0} \end{pmatrix} = \begin{pmatrix} \mathbf{0} & -\boldsymbol{\sigma}^2 \\ \boldsymbol{\sigma}^2 & \mathbf{0} \end{pmatrix}. \quad (53)$$

The principal equation Eq. 42, simplifies for the two-dimensional incompressible flow and is given by:

$$\text{tr} [\underline{\boldsymbol{\sigma}}_{\text{local}}^{\mathbf{C}}(\mathbf{r})] = \frac{2}{3}Re_c^{-1} \bar{\mathbf{Q}}_{\mathbf{a}}(\mathbf{r}) \underline{\mathbf{f}}^{\mathbf{b}} \underline{D}_b (v_1(\mathbf{r}) \underline{\mathbf{Q}}^{\mathbf{a}}(\mathbf{r})) + \frac{1}{4} \mathbf{G}'_{\text{ab}}{}^{2\mathbf{D}}(\mathbf{r}) \mathbf{G}'_{2\mathbf{D}}{}^{\text{ab}}(\mathbf{r}), \quad (54)$$

with

$$\underline{\mathbf{f}}^{\mathbf{b}} \underline{D}_b v_1(\mathbf{r}) = \begin{pmatrix} \mathbf{f}^{\mathbf{b}} D_b v_1(\mathbf{r}) & 0 \\ 0 & -\mathbf{f}^{\mathbf{b}} D_b^* v_1^*(\mathbf{r}) \end{pmatrix}. \quad (55)$$

The first term on the right side of Eq. 54 has diagonal shape as discussed in Remark 4.

3.2 Block diagonal form

The field equation Eq. 54 can be rearranged in a way that on one hand $\underline{\mathbf{C}}$ gets a block diagonal form, and at the same time the subfields transforming equally under rotations are combined. This is possible because the rotations take diagonal shape (Eq. 46) and do not mix the individual components.

First, the diagonal term $\underline{\boldsymbol{\sigma}}_{\text{diag}}^{\mathbf{C}}(\mathbf{r})$ without coupling to the gauge fields is considered. Writing out the upper and lower blocks, its trace according to Eq. 54 is as follows ($i\mathbf{f}^{\mathbf{1}}\boldsymbol{\sigma}^2 = \boldsymbol{\sigma}^5$ in two dimensions according to Eq. 50):

$$\begin{aligned} \text{tr} [\underline{\boldsymbol{\sigma}}_{\text{diag}}^{\mathbf{C}}(\mathbf{r})] &= \frac{2}{3}Re_c^{-1} \begin{pmatrix} \mathbf{Q}_{\mathbf{a}}^{\dagger}(\mathbf{r}) & \mathbf{Q}_{\mathbf{a}}^{\mathbf{T}}(\mathbf{r}) \end{pmatrix} \begin{pmatrix} \mathbf{0} & i\mathbf{f}^{\mathbf{1}}\boldsymbol{\sigma}^2 \\ i\mathbf{f}^{\mathbf{1}}\boldsymbol{\sigma}^2 & \mathbf{0} \end{pmatrix} \begin{pmatrix} \mathbf{f}^{\mathbf{b}} \partial_b (v_1(\mathbf{r}) \mathbf{Q}^{\mathbf{a}}(\mathbf{r})) \\ \mathbf{f}^{\mathbf{b}} \partial_b (v_1^*(\mathbf{r}) \mathbf{Q}^{*\mathbf{a}}(\mathbf{r})) \end{pmatrix} \\ &= \frac{2}{3}Re_c^{-1} [\mathbf{Q}_{\mathbf{a}}^{\mathbf{T}}(\mathbf{r}) \boldsymbol{\sigma}^5 \mathbf{f}^{\mathbf{b}} \partial_b (v_1(\mathbf{r}) \mathbf{Q}^{\mathbf{a}}(\mathbf{r})) + \mathbf{Q}_{\mathbf{a}}^{\dagger}(\mathbf{r}) \boldsymbol{\sigma}^5 \mathbf{f}^{\mathbf{b}} \partial_b (v_1^*(\mathbf{r}) \mathbf{Q}^{*\mathbf{a}}(\mathbf{r}))]. \end{aligned} \quad (56)$$

Component-wise examination of Eq. 56 shows that the individual equations can be rearranged to produce two independent blocks:

$$\begin{aligned}
\text{tr}[\boldsymbol{\sigma}_{\text{diag}}^{\text{C}}(\mathbf{r})] &= \frac{2}{3}Re_c^{-1} \left[\begin{aligned} &\left(Q_{L,a}(\mathbf{r}) \quad Q_{R,a}(\mathbf{r}) \right) \boldsymbol{\sigma}^5 \mathbf{f}^b \partial_b \left(v_1(\mathbf{r}) \begin{pmatrix} Q_L^a(\mathbf{r}) \\ Q_R^a(\mathbf{r}) \end{pmatrix} \right) \\ &+ \left(Q_{L,a}^*(\mathbf{r}) \quad Q_{R,a}^*(\mathbf{r}) \right) \boldsymbol{\sigma}^5 \mathbf{f}^b \partial_b \left(v_1^*(\mathbf{r}) \begin{pmatrix} Q_L^{*a}(\mathbf{r}) \\ Q_R^{*a}(\mathbf{r}) \end{pmatrix} \right) \end{aligned} \right] \\
&= \frac{2}{3}Re_c^{-1} \left[\begin{aligned} &\left(Q_{L,a}^*(\mathbf{r}) \quad Q_{R,a}(\mathbf{r}) \right) \boldsymbol{\sigma}^5 \mathbf{f}^b \partial_b \left(\psi_1(\mathbf{r}) \begin{pmatrix} Q_L^a(\mathbf{r}) \\ Q_R^{*a}(\mathbf{r}) \end{pmatrix} \right) \\ &+ \left(Q_{L,a}(\mathbf{r}) \quad Q_{R,a}^*(\mathbf{r}) \right) \boldsymbol{\sigma}^5 \mathbf{f}^b \partial_b \left(\psi_1^*(\mathbf{r}) \begin{pmatrix} Q_L^{*a}(\mathbf{r}) \\ Q_R^a(\mathbf{r}) \end{pmatrix} \right) \end{aligned} \right] \\
&= \frac{2}{3}Re_c^{-1} \left[\begin{aligned} &\mathbf{Q}'_a{}^\dagger(\mathbf{r}) \boldsymbol{\sigma}^5 \mathbf{f}^b \partial_b (\psi_1(\mathbf{r}) \mathbf{Q}'^a(\mathbf{r})) \\ &+ \mathbf{Q}'_a{}^\text{T}(\mathbf{r}) \boldsymbol{\sigma}^5 \mathbf{f}^b \partial_b (\psi_1^*(\mathbf{r}) \mathbf{Q}'^{*a}(\mathbf{r})) \end{aligned} \right].
\end{aligned} \tag{57}$$

Where in the last step of Eq. 57, the projection fields \mathbf{Q}'^a were defined by swapping the respective lower entries of \mathbf{Q}^a and \mathbf{Q}^{*a} (Eq. 51):

$$\mathbf{Q}'^a(\mathbf{r}) = \begin{pmatrix} Q_L^a(\mathbf{r}) \\ Q_R^{*a}(\mathbf{r}) \end{pmatrix} \quad \mathbf{Q}'_a{}^\dagger(\mathbf{r}) = \left(Q_{L,a}^*(\mathbf{r}) \quad Q_{R,a}(\mathbf{r}) \right), \tag{58}$$

and

$$\psi_1(\mathbf{r}) = \begin{pmatrix} v_1(\mathbf{r}) & 0 \\ 0 & v_1^*(\mathbf{r}) \end{pmatrix}. \tag{59}$$

In this way, each of the two-component fields \mathbf{Q}'^a and \mathbf{Q}'^{*a} (Eq. 58) separately forms an equation with individually adjoint projection fields already:

$$\text{tr}[\boldsymbol{\sigma}_{\text{diag}}^{\text{C}}(\mathbf{r})] = \frac{1}{2} \text{tr}[\boldsymbol{\sigma}'_{\text{diag}}{}^{\text{C}}(\mathbf{r})] + \frac{1}{2} \text{tr}[\boldsymbol{\sigma}'_{\text{diag}}{}^{\text{C}}(\mathbf{r})], \tag{60}$$

with sub-components:

$$\text{tr}[\boldsymbol{\sigma}'_{\text{diag}}{}^{\text{C}}(\mathbf{r})] = \frac{4}{3}Re_c^{-1} \bar{\mathbf{Q}}'_a(\mathbf{r}) \mathbf{f}^b \partial_b (\psi_1(\mathbf{r}) \mathbf{Q}'^a(\mathbf{r})). \tag{61}$$

$$\text{tr}[\boldsymbol{\sigma}'_{\text{diag}}{}^{\text{C}}(\mathbf{r})] = \frac{4}{3}Re_c^{-1} \bar{\mathbf{Q}}'^*_a(\mathbf{r}) \mathbf{f}^b \partial_b (\psi_1^*(\mathbf{r}) \mathbf{Q}'^{*a}(\mathbf{r})), \tag{62}$$

and defining:

$$\bar{\mathbf{Q}}'_a(\mathbf{r}) = \mathbf{Q}'_a{}^\dagger(\mathbf{r}) \boldsymbol{\sigma}^5. \tag{63}$$

3.2.1 Insertion Again, the gauge fields are added to Eqs. 61 and 62. To do so, the lower entries of the respective rotational fields are swapped. This interchange of the lower entries of the generators of rotations Eq. 45 results in separating the left-handed and right-handed rotational components:

$$\mathbf{L}'^3 = \frac{1}{2}\mathbf{I} \quad \text{and} \quad \mathbf{L}'^3 = -\frac{1}{2}\mathbf{I}. \quad (64)$$

These generators lead to rotational fields of the form $e^{\frac{i}{2}\phi_3(\mathbf{r})\mathbf{I}}$ as well as $e^{-\frac{i}{2}\phi_3(\mathbf{r})\mathbf{I}}$ for the mirrored term, and have the transformation behavior of half-integer phase fields with respective reversed phase. This has the advantage that the rotations can be formulated as actual $U(1)$ fields with scalar generator. For this purpose, the fields are to be defined with integer generator, which in principle corresponds to a trace formation of the generators from Eq. 64. One obtains for the rotations:

$$\mathbf{R}'(\mathbf{r}) = \text{tr} \left[e^{\frac{i}{2}\phi_3(\mathbf{r})\mathbf{I}} \right] = e^{i\phi_3(\mathbf{r})} \quad \text{and} \quad \mathbf{R}'(\mathbf{r}) = \text{tr} \left[e^{-\frac{i}{2}\phi_3(\mathbf{r})\mathbf{I}} \right] = e^{-i\phi_3(\mathbf{r})}, \quad (65)$$

and for the vector potential (from Eq. 47):

$$\mathbf{A}'_{\perp}{}^{\mathbf{U}1} = \nabla\phi(\mathbf{r})\frac{1}{2}\text{tr}(\mathbf{I}) = \nabla\phi(\mathbf{r}). \quad (66)$$

The doubled generators halve the coupling constant compared to Eq. 48 and it holds for the covariant derivative:

$$\mathbf{D} = \nabla - ig_{U1}\mathbf{A}'_{\perp}{}^{\mathbf{U}1} \quad g_{U1} = \frac{g_{2D}}{2} = \frac{3}{4\sqrt{2}}\sqrt{Re_C}. \quad (67)$$

The components of the projection fields from Eq. 58 can now be specified as well:

$$\mathbf{Q}'^{\mathbf{a}}(\mathbf{r}) = \begin{pmatrix} Q'_L{}^{\mathbf{a}}(\mathbf{r}) \\ Q'^{*a}(\mathbf{r}) \end{pmatrix} = \mathbf{f}^1\mathbf{R}'(\mathbf{r})\mathbf{e}^{\mathbf{a}} = \mathbf{f}^1 e^{i\phi(\mathbf{r})}\mathbf{e}^{\mathbf{a}}. \quad (68)$$

Inserted and summarized, this gives for the block diagonal local stress tensor (from Eq. 54):

$$\text{tr} [\boldsymbol{\sigma}'_{\text{local}}{}^{\mathbf{C}}(\mathbf{r})] = \frac{4}{3}Re_C^{-1}\bar{\mathbf{Q}}'_{\mathbf{a}}(\mathbf{r})\mathbf{f}^{\mathbf{b}}D_b(v_1(\mathbf{r})\mathbf{Q}'^{\mathbf{a}}(\mathbf{r})) + \frac{1}{4}\mathbf{G}'_{\mathbf{ab}}{}^{\mathbf{U}1}(\mathbf{r})\mathbf{G}'_{\mathbf{U}1}{}^{\mathbf{ab}}(\mathbf{r}). \quad (69)$$

$$\text{tr} [\boldsymbol{\sigma}'_{\text{local}}{}^{\mathbf{C}}(\mathbf{r})] = \frac{4}{3}Re_C^{-1}\bar{\mathbf{Q}}'^{*}{}_{\mathbf{a}}(\mathbf{r})\mathbf{f}^{\mathbf{b}}D_b^*(v_1^*(\mathbf{r})\mathbf{Q}'^{*\mathbf{a}}(\mathbf{r})) + \frac{1}{4}\mathbf{G}'_{\mathbf{ab}}{}^{\mathbf{U}1}(\mathbf{r})\mathbf{G}'_{\mathbf{U}1}{}^{\mathbf{ab}}(\mathbf{r}). \quad (70)$$

The lower equation does not contain any additional information, therefore only the upper block (Eq. 69) is considered in the further argumentation.

3.3 Normalization

The scattering theory only treats those cases in which an actual scattering event takes place. This means that the projection fields $\mathbf{Q}'^a(\mathbf{r})$ are limited to those positions where particles are located, while otherwise they are zero. Hence, using definition Eq. 68, at a position \mathbf{r} it is valid that:

$$\mathbf{Q}'_a^\dagger(\mathbf{r})\mathbf{Q}'^a(\mathbf{r}) = \begin{cases} 2 & \text{particle at position } \mathbf{r}. \\ 0 & \text{otherwise.} \end{cases} \quad (71)$$

It is useful to redesign the normalization in such a way that, on one hand, the particle density and thus the geometric effective cross section is taken into account, and on the other hand the projection fields are defined as continuous functions over the whole space. To achieve this, some average quantities for air molecules are introduced. These are given by:

- The average diameter of an air particle $2r_p^{SI}$.
- The distance to the next particle, given by the mean free path d_{box}^{SI} .

Both are quantities for which experimental data is available in numerous cases (see Section 5.5). Based on this, the dimensionless box length d_c is defined:

$$d_c = \frac{d_{box}^{SI}}{2r_p^{SI}}. \quad (72)$$

As a model, the flow is conceived as a periodic distribution of air particles of diameter $2r_p^{SI}$. To achieve periodicity, each particle occupies a square box of length $\frac{\sqrt{\pi}}{2}d_{box}^{SI}$, which contains the same area as a circle of diameter d_{box}^{SI} (Fig. 3a). For the theory, only the ratios between the quantities are crucial, so for the sake of simplicity, the particles are also assumed to be quadratic (Fig. 3b).

For the volume integral of the projection fields over a box, taking into account Eq. 71, it holds that:

$$\int_{V_{box}} \mathbf{Q}'_a^\dagger(\mathbf{r})\mathbf{Q}'^a(\mathbf{r})d\mathbf{r} = \int_{V_p} \mathbf{Q}'_a^\dagger(\mathbf{r})\mathbf{Q}'^a(\mathbf{r})dx_1dx_2 = 2(r_p^{SI})^2\pi. \quad (73)$$

Based on this, a fluid-wave function with new normalization is defined:

$$\psi'^a(\mathbf{r}) = d_c\sqrt{\frac{2}{\pi}}\mathbf{Q}'^a(\mathbf{r}). \quad (74)$$

Where d_c serves as a stretching factor and $\sqrt{\frac{2}{\pi}}$ as a form factor. The average of this wave function squared is given by (using Eq. 73):

$$(d_{box}^{SI})^{-2} \int_{V_{box}} \psi'_a{}^\dagger(\mathbf{r})\psi'^a(\mathbf{r})dV = 1, \quad (75)$$

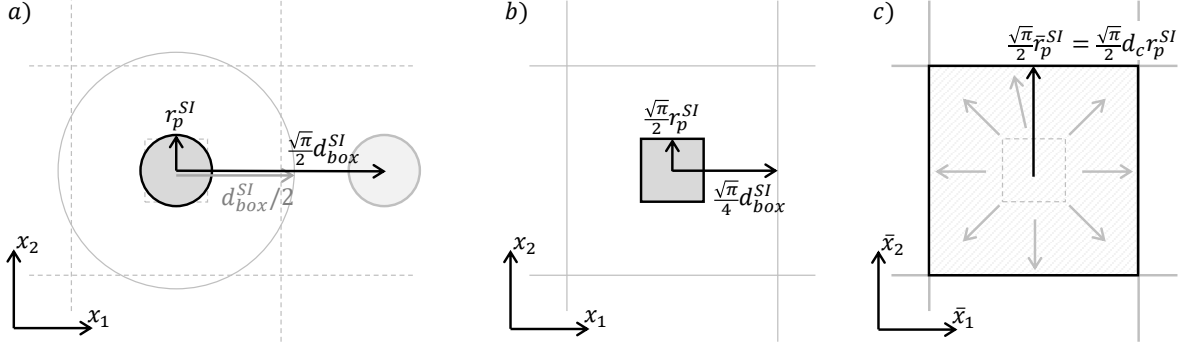


Figure 3: a) The cylindrical or circular air molecules with radius $2r_p^{SI}$ are periodically arranged in boxes with the same area as a circle with diameter of the mean free path d_{box}^{SI} . b) The air molecules are replaced by square areas of the same extension (form factor). c) To be able to define the projection functions on the whole space, the particles are distributed on the whole cell by means of stretched coordinates $\bar{r} = d_c r$, while at the same time the density of the state is reduced (stretch factor).

and corresponds to the average number of particles per box. Therefore, the normalization defined by Eq. 75 can be interpreted as follows:

The physical particle is stretched to the total volume of the box, while at the same time the density of the state is reduced by a factor d_c^{-2} , such that the state probability remains the same. The space is thus filled with particles, which, however, simulate the geometry of smaller particles due to their lower density of state (3c).

With this interpretation, the scattering quantities are defined on the entire volume (completeness), while at the same time the geometric cross section is taken into account by the stretching.

3.3.1 Insertion To define all quantities on the entire volume, in addition to the normalization Eq. 75, the field quantities are expressed with respect to stretched coordinates $\bar{\mathbf{r}}$, where it holds that:

$$\bar{\mathbf{r}} = d_c \mathbf{r} \quad \psi'^{\mathbf{a}}(\bar{\mathbf{r}}) = \psi'^{\mathbf{a}}(\mathbf{r}) \quad v_1(\bar{\mathbf{r}}) = v_1(\mathbf{r}). \quad (76)$$

When inserting into equation Eq. 69, the field differentials must also be transformed. One obtains for a vector field $\mathbf{w}(\bar{\mathbf{r}})$:

$$\nabla \mathbf{w}(\bar{\mathbf{r}}) = \frac{\partial \mathbf{w}(\bar{\mathbf{r}})}{\partial \mathbf{r}} = \frac{\partial \mathbf{w}(\bar{\mathbf{r}})}{\partial \bar{\mathbf{r}}} \frac{\partial \bar{\mathbf{r}}}{\partial \mathbf{r}} = d_c \bar{\nabla} \mathbf{w}(\bar{\mathbf{r}}). \quad (77)$$

Inserting the fluid wave function Eq. 74 into Eq. 69 and expressed with respect to the stretched coordinates yields:

$$\text{tr} [\boldsymbol{\sigma}'_{\text{local}}(\bar{\mathbf{r}})] = \frac{2\pi}{3} (Re_c d_c)^{-1} \bar{\psi}'_{\mathbf{a}}(\bar{\mathbf{r}}) \mathbf{f}^{\mathbf{b}} \bar{D}_{\mathbf{b}} (v_1(\bar{\mathbf{r}}) \psi'^{\mathbf{a}}(\bar{\mathbf{r}})) + \frac{1}{4} \mathbf{G}'_{\mathbf{ab}} \mathbf{U}_1(\bar{\mathbf{r}}) \mathbf{G}'_{\mathbf{U}_1}(\bar{\mathbf{r}}). \quad (78)$$

With wave functions (Eq. 68 inserted into 74):

$$\boldsymbol{\psi}'^{\mathbf{a}}(\bar{\mathbf{r}}) = \begin{pmatrix} \psi_L^{\mathbf{a}}(\mathbf{r}) \\ \psi_R^{*\mathbf{a}}(\mathbf{r}) \end{pmatrix} = d_c \sqrt{\frac{2}{\pi}} \mathbf{Q}'_{\mathbf{a}} = d_c \sqrt{\frac{2}{\pi}} \mathbf{f}^1 \mathbf{R}'(\bar{\mathbf{r}}) \mathbf{e}^{\mathbf{a}} = d_c \sqrt{\frac{2}{\pi}} \mathbf{f}^1 e^{i\phi(\bar{\mathbf{r}})} \mathbf{e}^{\mathbf{a}}, \quad (79)$$

and (applying Eq. 63):

$$\bar{\boldsymbol{\psi}}'_{\mathbf{a}}(\bar{\mathbf{r}}) = d_c \sqrt{\frac{2}{\pi}} \bar{\mathbf{Q}}'_{\mathbf{a}} = \boldsymbol{\psi}'_{\mathbf{a}}{}^{\dagger}(\bar{\mathbf{r}}) \boldsymbol{\sigma}^5 = d_c \sqrt{\frac{2}{\pi}} \mathbf{e}_{\mathbf{a}} e^{-i\phi(\bar{\mathbf{r}})} \mathbf{f}_1 \boldsymbol{\sigma}^5. \quad (80)$$

As well as the covariant derivative with respect to the stretched coordinates (Eq. 77 inserted into Eq. 67):

$$\bar{\mathbf{D}} = \bar{\nabla} - ig_{U1} \mathbf{A}'_{\perp}{}^{\mathbf{U}1}(\bar{\mathbf{r}}) \quad \mathbf{A}'_{\perp}{}^{\mathbf{U}1}(\bar{\mathbf{r}}) = \bar{\nabla} \phi(\bar{\mathbf{r}}). \quad (81)$$

3.4 Initial state: Laminar boundary layer

3.4.1 Basic parameters in the laminar boundary layer Up to the point of emergence of the TS waves, the fluid can be modeled as a laminar Blasius boundary layer flow with the relative height expressed as a self-similar variable η (Blasius, 1908):

$$\eta(\bar{\mathbf{r}}) = x_2^{SI} \sqrt{\frac{\rho^{SI} v_{\infty}^{SI}}{\mu^{SI} x_1^{SI}}} = \frac{\bar{x}_2}{\bar{x}_1} \sqrt{Re_{\infty}} \quad \text{with} \quad \bar{\mathbf{r}} = (\bar{x}_1, \bar{x}_2). \quad (82)$$

Here Re_{∞} denotes the Reynolds number at infinite distance from the plate surface, expressed with respect to the dimensionless stretched coordinate \bar{x}_1 :

$$Re_{\infty} = \frac{\rho^{SI} v_{\infty}^{SI} x_1^{SI}}{\mu^{SI}} = \frac{\rho^{SI} v_{\infty}^{SI} d_c}{\mu^{SI}} \bar{x}_1. \quad (83)$$

3.4.2 Effective shear For the model being developed, it appears that the velocity profile is of interest in the region near the plate surface, where it behaves as a parallel shear flow (Fig. 4a). In this region, the velocity field can be expressed as a linearly approximated function of height η (according to Eq. 82):

$$v_1(\bar{\mathbf{r}}) \approx 0.332 \eta(\bar{\mathbf{r}}) = 0.332 \frac{\bar{x}_2}{\bar{x}_1} \sqrt{Re_{\infty}} = c_1 \frac{\bar{x}_2}{\bar{x}_1} \sqrt{Re_{\infty}}. \quad (84)$$

The approximated linear velocity profile is shown in Fig. 4a with a gray line. From here on, we write for the coefficient $c_1 = 0.332$ and calculate the velocity gradient applied to the particle:

$$\begin{aligned} \mathbf{f}^2 \bar{\partial}_2 v_1(\bar{\mathbf{r}}) + \mathbf{f}^1 \bar{\partial}_1 v_1(\bar{\mathbf{r}}) &= \mathbf{f}^2 \frac{c_1}{\bar{x}_1} \sqrt{Re_{\infty}} - \mathbf{f}^1 \frac{c_1 \bar{x}_2}{2(\bar{x}_1)^2} \sqrt{Re_{\infty}} \\ &\approx \mathbf{f}^2 \frac{c_1}{\bar{x}_1} \sqrt{Re_{\infty}} = \mathbf{f}^2 \omega_{eff}. \end{aligned} \quad (85)$$

In the approximation it was used that in the boundary layer the distance to the plate surface is small ($x_2 = \frac{x_2^{SI}}{l_c} \ll 1$) and thus the derivative in \bar{x}_1 -direction (second term in Eq. 85) is much smaller than the derivative in \bar{x}_2 direction (first term in Eq. 85). The amount of shear effectively acting on the particle is given by:

$$\omega_{eff.} = \frac{c_1}{\bar{x}_1} \sqrt{Re_\infty}. \quad (86)$$

Remark 6 *Since the gradient Eq. 85 is performed with respect to the stretched coordinates \bar{x}_1, \bar{x}_2 , the expression for $\omega_{eff.}$ (Eq. 86) includes only the fraction of the velocity difference which acts on the actual particle, i.e. the effective velocity difference.*

3.4.3 Velocity field in a box The scattering theory will be defined along a line of constant velocity $v^{SI} = v_\infty^{SI} v$, corresponding to a constant relative height $\eta^0 = const.$ in the velocity profile.

Since the scattering processes occur within a small box, the velocity field is of interest only at a fixed height \bar{x}_2^0 with a small deviation (Fig. 4b):

$$\bar{x}'_2 = \bar{x}_2 - \bar{x}_2^0. \quad (87)$$

The relative height (Eq. 82) can be expressed with respect to these shifted coordinates according to:

$$\eta(\bar{\mathbf{r}}) = \eta^0 + \eta'(\bar{\mathbf{r}}) \quad \eta^0 = \frac{\bar{x}_2^0}{\bar{x}_1} \sqrt{Re_\infty} \quad \eta'(\bar{\mathbf{r}}) = \frac{\bar{x}'_2}{\bar{x}_1} \sqrt{Re_\infty}. \quad (88)$$

Finally it holds for the real velocity field (Eq. 88 inserted into Eq. 84):

$$v_1(\bar{\mathbf{r}}) = v_1^*(\bar{\mathbf{r}}) = v + c_1 \eta'(\bar{\mathbf{r}}) = v + \bar{x}'_2 \omega_{eff.}, \quad (89)$$

where

$$v = c_1 \eta^0 = const. \quad (90)$$

Therefore, for the flow in a box along the line considered (Eq. 89), one obtains a constant base flow $v = const.$ as well as a small shear component $\omega_{eff.}$. This corresponds to the form required for the construction according to Par. 2.2.1 and can be inserted into the stress tensor Eq. 78.

3.4.4 Insertion When inserting the velocity field Eq. 89, it is utilized that the field is real, and thus it holds that:

$$v_1(\bar{\mathbf{r}}) = \begin{pmatrix} v_1(\bar{\mathbf{r}}) & 0 \\ 0 & v_1^*(\bar{\mathbf{r}}) \end{pmatrix} = \mathbf{I}v_1(\bar{\mathbf{r}}). \quad (91)$$

Thus, the velocity field can be inserted into Eq. 78, with the velocity gradient according to Eq. 85 executed explicitly. Again, the diagonal term σ'_{diag} is considered first:

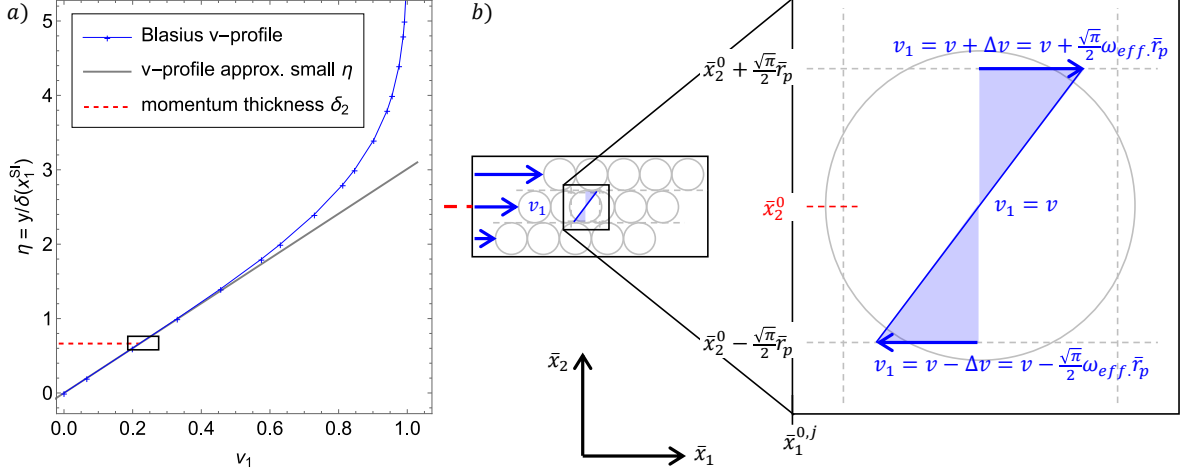


Figure 4: a) Nondimensionalized velocity profile in the laminar boundary layer. In blue the numerically calculated Blasius velocity profile (values used from Jaman, Molla & Sultana, 2011). In gray, the linearly approximated velocity profile for small η . (b) Schematic illustration of the layers and details within an elementary cell including the definition of the coordinates. The top and bottom layers move faster/ slower by a velocity amount of $\pm\Delta v = \pm\frac{\sqrt{\pi}}{2}\omega_{eff}.\bar{r}_p$ than the cell under consideration.

$$\begin{aligned}
\text{tr}[\boldsymbol{\sigma}'_{\text{diag}}(\bar{\mathbf{r}})] &= \frac{2\pi}{3}(Re_c d_c)^{-1} \bar{\boldsymbol{\psi}}'_a(\bar{\mathbf{r}}) \mathbf{f}^b \bar{\partial}_b \left(v_1(\bar{\mathbf{r}}) \boldsymbol{\psi}'^a(\bar{\mathbf{r}}) \right) \\
&= \frac{2\pi}{3}(Re_c d_c)^{-1} \bar{\boldsymbol{\psi}}'_a(\bar{\mathbf{r}}) \left[\mathbf{f}^b \bar{\partial}_b \left(v_1(\bar{\mathbf{r}}) \right) \boldsymbol{\psi}'^a(\bar{\mathbf{r}}) + v_1(\bar{\mathbf{r}}) \mathbf{f}^b \bar{\partial}_b \left(\boldsymbol{\psi}'^a(\bar{\mathbf{r}}) \right) \right] \\
&\approx \frac{2\pi}{3}(Re_c d_c)^{-1} \bar{\boldsymbol{\psi}}'_a(\bar{\mathbf{r}}) \left[\mathbf{f}^2 \omega_{eff} \boldsymbol{\psi}'^a(\bar{\mathbf{r}}) + (v + \bar{x}'_2 \omega_{eff}) \mathbf{f}^b \bar{\partial}_b \left(\boldsymbol{\psi}'^a(\bar{\mathbf{r}}) \right) \right] \quad (92) \\
&\approx \frac{2\pi}{3}(Re_c d_c)^{-1} \bar{\boldsymbol{\psi}}'_a(\bar{\mathbf{r}}) \left[\mathbf{f}^2 \omega_{eff} \boldsymbol{\psi}'^a(\bar{\mathbf{r}}) + v \mathbf{f}^b \bar{\partial}_b \left(\boldsymbol{\psi}'^a(\bar{\mathbf{r}}) \right) \right] \\
&= \frac{2\pi}{3}(Re_c d_c)^{-1} \bar{\boldsymbol{\psi}}'_a(\bar{\mathbf{r}}) \left(\mathbf{f}^2 \omega_{eff} + v \mathbf{f}^b \bar{\partial}_b \right) \boldsymbol{\psi}'^a(\bar{\mathbf{r}}).
\end{aligned}$$

In these steps, the approximation was such that in each order only the leading term was considered. In detail, the approximations are:

- consideration of the boundary layer near the surface, such that $x_2 = \frac{x_2^{SI}}{l_c} \ll 1$.
- consideration of a small enough box, such that $\bar{x}'_2 \omega_{eff} \ll v$.

3.4.5 Diagonalization of the shear term Since the shear in Eq. 92 is no longer dependent of \mathbf{f}^1 , the shear term $\mathbf{f}^2 \omega_{eff}$ can be diagonalized by means of a location-independent rotation \mathbf{R}_0 . Specifically, the following rotation is used:

$$\mathbf{R}_0 = e^{i\sigma^2 \pi/4}, \quad (93)$$

and inserted with the wave functions according to Eq. 79, the diagonalized shear term is obtained:

$$\begin{aligned}
\bar{\psi}'_{\mathbf{a}}(\bar{\mathbf{r}})\mathbf{f}^2\omega_{eff}\psi'^{\mathbf{a}}(\bar{\mathbf{r}}) &= \frac{2d_c^2}{\pi} \text{tr} [e^{-i\phi(\bar{\mathbf{r}})}\mathbf{f}_1\boldsymbol{\sigma}^5\mathbf{f}^2\omega_{eff}\mathbf{f}^1e^{i\phi(\bar{\mathbf{r}})}] \\
&= \frac{2d_c^2}{\pi} \text{tr} [\mathbf{R}_0^\dagger e^{-i\phi(\bar{\mathbf{r}})}\mathbf{f}_1\boldsymbol{\sigma}^5\mathbf{f}^2\omega_{eff}\mathbf{f}^1e^{i\phi(\bar{\mathbf{r}})}\mathbf{R}_0] \\
&= \frac{2d_c^2}{\pi} \text{tr} [e^{-i\phi(\bar{\mathbf{r}})}\mathbf{f}_1\boldsymbol{\sigma}^5(\mathbf{R}_0^\dagger\mathbf{f}^2\mathbf{R}_0^\dagger)\omega_{eff}\mathbf{f}^1e^{i\phi(\bar{\mathbf{r}})}] \\
&= \frac{2d_c^2}{\pi} \text{tr} [e^{-i\phi(\bar{\mathbf{r}})}\mathbf{f}_1\boldsymbol{\sigma}^5(i\mathbf{I})\omega_{eff}\mathbf{f}^1e^{i\phi(\bar{\mathbf{r}})}] \\
&= \bar{\psi}'_{\mathbf{a}}(\bar{\mathbf{r}})i\omega_{eff}\mathbf{I}\psi'^{\mathbf{a}}(\bar{\mathbf{r}}).
\end{aligned} \tag{94}$$

Thereby, the invariance of the trace under cyclic permutations and the anticommutation of $\boldsymbol{\sigma}^5$ with the Pauli matrices were used.

Remark 7 Please note that this procedure works only in the incompressible case with phase $\theta = 0$, since the rotation \mathbf{R}_0 would mix the phase components.

Substituting into the governing Eq. 78 results in:

$$\text{tr} [\boldsymbol{\sigma}'_{\text{local}}(\bar{\mathbf{r}})] = \frac{2\pi}{3}(Re_c d_c)^{-1} \bar{\psi}'_{\mathbf{a}}(\bar{\mathbf{r}}) \left(i\omega_{eff}\mathbf{I} + v\mathbf{f}^b\bar{D}_b \right) \psi'^{\mathbf{a}}(\bar{\mathbf{r}}) + \frac{1}{4}\mathbf{G}'_{\text{ab}}\mathbf{U}^1(\bar{\mathbf{r}})\mathbf{G}'_{\text{U}^1}{}^{\text{ab}}(\bar{\mathbf{r}}). \tag{95}$$

3.5 Locality and local Reynolds number

While the action of the applied fields is estimated locally, Re_c in Eq. 95 is a non-local constant and indirectly introduces a long-range interaction with the flow conditions at chord length l_c^{SI} of the airfoil.

This problem can be circumvented by using the local Reynolds number Re_L (e.g. Schlichting & Gersten 2017) instead of the characteristic Reynolds number Re_c (according to Eq. 3 in Part I) to nondimensionalize the Navier-Stokes equations:

$$Re_c = \frac{\rho^{SI}v_\infty^{SI}l_c^{SI}}{\mu^{SI}} \quad \longrightarrow \quad Re_L = \frac{\rho^{SI}v^{SI}x_1^{SI}}{\mu^{SI}}. \tag{96}$$

To do so, it is required that Re_L can be considered constant in the range of the scattering process, which takes place within a box of length $\frac{\sqrt{\pi}}{2}d_{box}^{SI}$ according to Par. 3.3.

This is the case in the boundary layer for $x_1^{SI} \gg d_{box}^{SI}$, since additionally in Par. 3.4, the influence of the velocity gradient inside the box has been separated from the velocity field. Thus, Eq. 95 is rescaled to:

$$\text{tr} [\boldsymbol{\sigma}'_{\text{local}}(\bar{\mathbf{r}})] = \frac{2\pi}{3}(Re_L d_c)^{-1} \bar{\psi}'_{\mathbf{a}}(\bar{\mathbf{r}}) \left(i\omega_{eff}\mathbf{I} + v\mathbf{f}^b\bar{D}_b \right) \psi'^{\mathbf{a}}(\bar{\mathbf{r}}) + \frac{1}{4}\mathbf{G}'_{\text{ab}}\mathbf{U}^1(\bar{\mathbf{r}})\mathbf{G}'_{\text{U}^1}{}^{\text{ab}}(\bar{\mathbf{r}}). \tag{97}$$

With local coupling to the phase field (see Eqs. 67 and 81):

$$\bar{\mathbf{D}} = \bar{\nabla} - ig_{U^1}^L \mathbf{A}'_{\perp}{}^{\text{U}^1}(\bar{\mathbf{r}}) \quad g_{U^1}^L = \frac{3}{4\sqrt{2}}\sqrt{Re_L}. \tag{98}$$

Remark 8 (Interpretation) *In detail, the coordinate along the plate is split into the starting coordinate of the box $x_1^{0,j}$ (see Fig. 4b) and the residual coordinate inside the box $x_1'^{SI}$:*

$$x_1^{SI} = x_1^{0,j} + x_1'^{SI}. \quad (99)$$

Thereby, $x_1^{0,j}$ is a dimensioned quantity, the superscript $()^{SI}$ is omitted for readability. For the nondimensionalization, the Reynolds number at the starting coordinate $x_1^{0,j}$ of the scattering box is used:

$$Re_L = \frac{\rho^{SI} v^{SI} x_1^{0,j}}{\mu^{SI}} \underset{x_1^{0,j} \gg d_{box}^{SI}}{\approx} \frac{\rho^{SI} v^{SI} x_1^{SI}}{\mu^{SI}}. \quad (100)$$

This nondimensionalization corresponds to a substitution of the length scale to (compare with Eq. 2 in Part I):

$$x_1 = \frac{x_1^{SI}}{x_1^{0,j}} = \frac{x_1^{0,j} + x_1'^{SI}}{x_1^{0,j}} = 1 + \frac{1}{j} \frac{x_1'^{SI}}{d_{box}^{SI}} \quad \nabla = x_1^{0,j} \nabla^{SI}. \quad (101)$$

Where the starting coordinate of the j -th box was expressed in terms of box lengths as $x_1^{0,j} = j \cdot d_{box}^{SI}$.

The periodic structure allows to limit the domain to a single box (which corresponds to superimposing previously traversed boxes):

$$x_1^{mod} = x_1 \bmod 1 = \frac{1}{j} \frac{x_1'^{SI}}{d_{box}^{SI}}. \quad (102)$$

In this form, the nondimensionalization of the length scale can be interpreted as the mean value of the nondimensionalized coordinate within the box $\frac{x_1'^{SI}}{d_{box}^{SI}}$, averaged over the number j of boxes traversed up to that point.

3.6 Quantization of the theory

3.6.1 Interpretation as Euclidean quantum theory Eq. 97 has the mathematical form of a Lagrangian for the two-dimensional Euclidean Dirac equation with normalized, explicitly $SO(2)$ -invariant wave functions $\psi'^a(\bar{\mathbf{r}})$ as solutions (see the formalism in van Nieuwenhuizen & Waldron 1996). This implies that Eq. 97 can be quantized using the formalism of second quantization by forming operators Ψ' from the wave functions:

$$\Psi'(\bar{\mathbf{r}}) = \sum_b \psi'^b(\bar{\mathbf{r}}) a_b. \quad (103)$$

In addition, the definition of boxes with periodic boundary conditions according to Section 3.3 is helpful, since these can be used as a natural cut-off criterion.

However, one can go even further – with a few more considerations, it is possible to formulate a fully quantized scattering theory starting from the current Euclidean field theory. The steps needed for this are carried out in this section:

First, a basic direction of time evolution is needed (Par. 3.6.2). Then the time component is Wick-rotated to obtain a covariant, dynamic quantum theory (Par. 3.6.4). To ensure that the resulting theory is unitary, reflection positivity of the Euclidean theory is shown in advance (Par. 3.6.3). Furthermore, the physical interpretation as a Lagrangian density is motivated (Par. 3.6.5).

In the transition from Euclidean to Minkowski space, Latin indices $a, b \in 1, 2$ are used for Euclidean quantities, and Greek indices $\alpha, \beta \in 0, 1$ for quantities in Minkowski space. Additionally, if the notation might be ambiguous, in this section $()_E$ and $()_M$ sub- or superscripts are inserted for Euclidean and Minkowski measures, respectively.

3.6.2 Basic time direction, mapping of the time- to the x_1 -axis The scattering theory is defined along a line of constant velocity $v^{SI} = v_\infty^{SI}v$, which corresponds to a constant relative height η (Eq. 82) in the velocity profile. Along this line, the local Reynolds number Re_L is only a function of the dimensionless coordinate in the profile direction $Re_L = Re_L(\bar{x}_1)$ in the incompressible case.

Both quantities Re_L and \bar{x}_1 are used to track the evolution of the flow along the plate (e.g., Figs. 1 & 2) and implicitly correspond through:

$$\bar{x}_1 = vt \tag{104}$$

to the time evolution of a fluid volume along constant relative height η . Eq. 104 defines a basic time axis with respect to which the scattering theory can be formulated.

3.6.3 Reflection positivity By defining a time axis according to Eq. 104, the wave functions Eq. 79 can be expressed as functions of time:

$$\psi'^{\mathbf{a}}(\bar{\mathbf{r}}) = \psi'^{\mathbf{a}}(vt, \bar{x}_2) \quad \text{with} \quad (d_{box}^{SI})^{-2} \int_{V_{box}} \psi'_{\mathbf{a}}{}^\dagger(vt, \bar{x}_2) \psi'^{\mathbf{a}}(vt, \bar{x}_2) dV = 1, \tag{105}$$

additionally, the inner product is defined as follows:

$$\langle \psi', \phi' \rangle_E = (d_{box}^{SI})^{-2} \int_{V_{box}} \bar{\psi}'_{\mathbf{a}} \phi'^{\mathbf{a}} dV = (d_{box}^{SI})^{-2} \int_{V_{box}} \psi'_{\mathbf{a}}{}^\dagger \sigma^5 \phi'^{\mathbf{a}} dV. \tag{106}$$

Reflection positivity for the functions Eq. 105 with respect to the inner product Eq. 106 is given if it holds that (see e.g. Friedli & Velenik, 2017; Neeb & Ólafsson, 2018):

$$\langle \psi'(vt, \bar{x}_2), \psi'(-vt, \bar{x}_2) \rangle_E \geq 0 \quad t \in [0, \infty). \tag{107}$$

To show that condition Eq. 107 is satisfied, the explicit forms of the wave functions can be used. These are defined by (Eq. 79):

$$\psi'^{\mathbf{a}}(vt, \bar{x}_2) = \begin{pmatrix} \psi_L^{\mathbf{a}}(vt, \bar{x}_2) \\ \psi_R^{*\mathbf{a}}(vt, \bar{x}_2) \end{pmatrix} = d_c \sqrt{\frac{2}{\pi}} \mathbf{f}^{\mathbf{1}} e^{i\phi(vt, \bar{x}_2)} \mathbf{e}^{\mathbf{a}}. \tag{108}$$

Where ψ_L and ψ_R^* transform equally under rotations (however the sign of the phase θ would be reversed). Under time inversion, the generator of rotations changes its sign $\mathbf{L}_3 \xrightarrow{-t} -\mathbf{L}_3$, which means for the rotation angle that:

$$\phi(-vt, \bar{x}_2) = -\phi(vt, \bar{x}_2), \quad (109)$$

and for the time-inverted wave functions (Eq. 109 inserted into Eq. 108):

$$\psi'^{\mathbf{a}}(-vt, \bar{x}_2) = \begin{pmatrix} \psi_L^{\mathbf{a}}(-vt, \bar{x}_2) \\ \psi_R^{*\mathbf{a}}(-vt, \bar{x}_2) \end{pmatrix} = d_c \sqrt{\frac{2}{\pi}} \mathbf{f}^{\mathbf{1}} e^{-i\phi(vt, \bar{x}_2)} \mathbf{e}^{\mathbf{a}}. \quad (110)$$

With this, the condition for reflection positivity Eq. 107 can be verified by explicit calculation:

$$\begin{aligned} \langle \psi'(vt, \bar{x}_2), \psi'(-vt, \bar{x}_2) \rangle_E &= (d_{box}^{SI})^{-2} \int_{V_{box}} \left[-\psi_a^{*L}(vt, \bar{x}_2) \psi_L^{\mathbf{a}}(-vt, \bar{x}_2) \right. \\ &\quad \left. + \psi_a^R(vt, \bar{x}_2) \psi_R^{*\mathbf{a}}(-vt, \bar{x}_2) \right] dV \\ &= (\sqrt{2\pi} r_p^{SI})^{-2} \int_{V_{box}} [-e^{-2i\phi(vt, \bar{x}_2)} + e^{-2i\phi(vt, \bar{x}_2)}] dV \\ &= 0. \end{aligned} \quad (111)$$

Eq. 111 satisfies condition Eq. 107 and shows that reflection positivity for wave functions Eq. 105 with the inner product Eq. 106 is given.

This is important because, according to the Osterwalder-Schrader theorem (Osterwalder & Schrader, 1973, 1975), a reflection-positive Euclidean field theory, when Wick-rotated, results in a unitary quantum field theory to which the common path integral formalism can be applied.

3.6.4 Time evolution and Wick rotation to a dynamic scattering theory The equation for the stress tensor Eq. 97 involves compact Lie groups only, and is therefore analytically continuable (Chevalley complexification). Thus, the time coordinate can be Wick-rotated and restricted to complex values (Wick, 1954):

$$\bar{x}_1 \longrightarrow ivt \quad t \in \mathbb{R}. \quad (112)$$

The Wick rotation for the Clifford algebra is nontrivial, and can be carried out using the mechanism presented in van Nieuwenhuizen & Waldron (1996). This leads to a rotation of $i\sigma_{\mathbf{E}}^5$ (Eq. 50) onto the basis vector $\mathbf{f}_{\mathbf{M}}^{\mathbf{0}}$. Together with the conversion of the Euclidean indices from $a, b \in \{1, 2\}$ to the counting method in Minkowski space with $\alpha, \beta \in \{0, 1\}$ this yields for the Euclidean basis vectors $\mathbf{f}_{\mathbf{E}}^{\mathbf{k}}$ (Eq. 44) when transformed to the Minkowski basis $\mathbf{f}_{\mathbf{M}}^{\mathbf{k}}$:

$$\begin{aligned}
i\sigma_{\mathbf{E}}^5 &\longrightarrow \mathbf{f}_{\mathbf{M}}^0 = \gamma^0 = \begin{pmatrix} -i & 0 \\ 0 & i \end{pmatrix} \\
\mathbf{f}_{\mathbf{E}}^1 &\longrightarrow \mathbf{f}_{\mathbf{M}}^1 = \gamma^1 = \begin{pmatrix} 0 & 1 \\ 1 & 0 \end{pmatrix},
\end{aligned} \tag{113}$$

with $(\gamma^0\gamma^0) = -\mathbf{I}$ and $(\gamma^1\gamma^1) = \mathbf{I}$, which corresponds to a rotation into the Minkowski space with metric tensor $g_{\alpha\beta} = \text{diag}(-1, +1)$.

The transformation rules for the further objects are:

$$\begin{aligned}
\psi'^a &\longrightarrow \psi^\alpha \\
\bar{\psi}'_a = \psi'^{\dagger}_a \sigma^5 &\longrightarrow -\psi^\dagger_\alpha i\gamma^0 = -\bar{\psi}_\alpha \\
\sigma'_{\text{local}} &\longrightarrow \sigma_{\text{local}}^{\mathbf{M}} \\
\mathbf{G}'_{\text{ab}}{}^{\mathbf{U1}} \mathbf{G}'_{\mathbf{U1}}{}^{\text{ab}} &\longrightarrow -\mathbf{G}_{\alpha\beta} \mathbf{G}^{\alpha\beta} \\
i\omega_{\text{eff.}} = i \frac{c_1}{\bar{x}_1} \sqrt{Re_\infty} &\longrightarrow \frac{c_1}{vt} \sqrt{Re_\infty} = \frac{c_1}{\bar{x}_0^{\mathbf{M}}} \sqrt{Re_\infty} = \omega_{\text{eff.}}.
\end{aligned} \tag{114}$$

Please note that the i in the shear term $\omega_{\text{eff.}}$ vanishes upon Wick rotation due to the dependence on \bar{x}_1 . For Eq. 97, the Wick-rotated form is obtained:

$$\text{tr} [\sigma_{\text{local}}^{\mathbf{M}}(\bar{\mathbf{r}})] = -\frac{2\pi}{3} (Re_L d_c)^{-1} \bar{\psi}_\alpha(\bar{\mathbf{r}}) \left(\mathbf{I} \omega_{\text{eff.}} + v \gamma^\beta \bar{D}_\beta \right) \psi^\alpha(\bar{\mathbf{r}}) - \frac{1}{4} \mathbf{G}_{\alpha\beta}(\bar{\mathbf{r}}) \mathbf{G}^{\alpha\beta}(\bar{\mathbf{r}}). \tag{115}$$

As well as the Wick-rotated inner product:

$$\langle \psi, \phi \rangle_M = (d_{\text{box}}^{SI})^{-2} \int_{V_{\text{box}}} \bar{\psi} \phi dV = (d_{\text{box}}^{SI})^{-2} \int_{V_{\text{box}}} \psi^\dagger \gamma^0 \phi dV. \tag{116}$$

With the Wick rotation, a relativistically covariant time evolution is introduced. This aspect is further elaborated in the discussion (Par. 6.2).

3.6.5 Equation of momentum density and interpretation as Lagrangian density The gradient of the stress tensor in Euclidean space by definition represents a force density \mathbf{f} (e.g. Eq. 5 in Part I), written in components $\bar{\partial}_j \sigma_{jk}^E = f_k^E$.

With Wick rotation, the 0.-th spatial coordinate becomes the time coordinate. Thus, in Minkowski space it holds that $\bar{\partial}_0 \sigma_{0k}^M = v^{-1} \bar{\partial}_t \sigma_{0k}^M = f_k^M$. Therefore $v^{-1} \sigma_{0k}^M$ is a quantity whose time derivative forms a force density. On the other hand, by conservation of momentum, a force density is equal to the time derivative of a momentum density ($\dot{\mathbf{p}} = \mathbf{f}$), which means in consequence that $v^{-1} \sigma_{0k}^M = p$ can be interpreted as Wick-rotated momentum density.

This interpretation can be extended to all components of $\sigma_{\text{local}}^{\mathbf{M}}$ if one considers that in the initial state only the 0.-th component contributes and the further components arise from this momentum-like state by rotations.

For the case of constant velocity trajectories, one obtains the generalized momentum density $p(\bar{\mathbf{r}})$ (Inserted from Eq. 115 and with $k_{eff.} = v^{-1}\omega_{eff.}$):

$$\begin{aligned} p(\bar{\mathbf{r}}) &= v^{-1}\text{tr} [\boldsymbol{\sigma}_{\text{local}}^{\text{M}}(\bar{\mathbf{r}})] \\ &= -\frac{2\pi}{3}(Re_L d_c)^{-1}\bar{\boldsymbol{\psi}}_{\alpha}(\bar{\mathbf{r}})\left(\mathbf{I}k_{eff.} + \gamma^{\beta}\bar{D}_{\beta}\right)\boldsymbol{\psi}^{\alpha}(\bar{\mathbf{r}}) - \frac{1}{4}v^{-1}\mathbf{G}_{\alpha\beta}(\bar{\mathbf{r}})\mathbf{G}^{\alpha\beta}(\bar{\mathbf{r}}) \quad (117) \\ &= \mathcal{L}(\bar{\mathbf{r}}). \end{aligned}$$

Where in the last step of Eq. 117 it is used that the expression is a tensor density and contains the information on the local momentum p of the system, which allows it to be interpreted as the root of a Lagrangian density. This is again equivalent to the interpretation as Lagrangian density \mathcal{L} if trajectories along constant flow velocity are considered (Rizzuti, Vasconcelos & Resende, 2019).

With this, the presented theory on fluid mechanics is put into a form which allows a direct interpretation as a scattering theory, and to which the known mathematical principles and solution approaches of quantum field theory can be applied.

4 First-order scattering theory for two-dimensional incompressible flows

With Eq. 117, a covariant field equation is developed, for which a quantized scattering theory can be established (Osterwalder & Schrader, 1973, 1975). In this section the details of the scattering theory are formulated.

The governing equation and the associated auxiliary quantities are summarized briefly in Par. 4.1.1 for convenience. Then the individual terms of the equation are considered separately and interpreted as laminar and vortical quasiparticles and their interactions. The properties of the quasiparticles are identified and the corresponding Green's functions (propagators) are specified.

From this, invariant scattering amplitudes and cross sections are determined using Feynman technology. The whole treatment is conducted as analogously as possible to the standard literature, with adjustments where necessary. The main source for definitions and basic quantities is Burgess & Moore (2006), which uses the same overall metric sign as this manuscript. The calculation is performed analogously to Peskin & Schroeder (1995) and Chiochia, Dissertori & Gehrman (2010), with individual steps in the calculation of the effective cross section adapted from the very detailed solutions in Lawson (2014) and Millar (2014).

4.1 Basic quantities of the scattering theory

4.1.1 Governing equation, coupling constant and fluid quantum of action The treatment of the scattering theory is based on Eq. 117, which has the form of a Lagrangian density for a two-dimensional Dirac equation. This is emphasized by adapting the nomenclature to standard quantum field theory:

$$\mathcal{L}(\bar{\mathbf{r}}) = -\bar{\boldsymbol{\psi}}_{\alpha}(\bar{\mathbf{r}})\left(\mathbf{I}m_{eff.} + \hbar_{fl}\bar{\boldsymbol{D}}\right)\boldsymbol{\psi}^{\alpha}(\bar{\mathbf{r}}) - \frac{1}{4}v^{-1}\mathbf{G}_{\alpha\beta}(\bar{\mathbf{r}})\mathbf{G}^{\alpha\beta}(\bar{\mathbf{r}}). \quad (118)$$

By comparing Eq. 118 with Eq. 117, the quantized fluid measures are defined. The fluid quantum of action \hbar_{fl} is given by:

$$\hbar_{fl} = \frac{2\pi}{3}(Re_L d_c)^{-1} = \frac{2\pi}{3}(Re_C v \bar{x}_0^M)^{-1}, \quad (119)$$

the effective mass m_{eff} , which is an auxiliary quantity to approximate the local velocity gradient in the initial laminar boundary layer, reads:

$$m_{eff} = \hbar_{fl} k_{eff} = \frac{2\pi}{3} \frac{c_1}{Re_L d_c v \bar{x}_0^M} \sqrt{Re_\infty}, \quad (120)$$

and accordingly the effective wavenumber is (definition in Par. 3.6.5):

$$k_{eff} = v^{-1} \omega_{eff} = c_1 (v \bar{x}_0^M)^{-1} \sqrt{Re_\infty}. \quad (121)$$

The underlying numerical parameters are determined according to their definitions in Par. 3.4 and Par. 3.3 for the dimensionless box radius d_c . The local Reynolds number Re_L is considered constant over a box ($x_0^M \gg d_{box}^{SI}$). The relations between the different Reynolds numbers introduced are:

$$Re_C = \frac{\rho^{SI} v_\infty^{SI} l_c^{SI}}{\mu^{SI}} \quad Re_\infty = \frac{Re_C}{d_c} \bar{x}_0^M \quad Re_L = \frac{Re_C v}{d_c} \bar{x}_0^M, \quad (122)$$

where Re_C denotes the characteristic Reynolds number (Eq. 3 in Part I), Re_∞ denotes the Reynolds number at infinite distance from the plate (Eq. 83) and Re_L the local Reynolds number (Eq. 96).

Furthermore, Feynman slash notation is used:

$$\bar{D} = \gamma^\beta \bar{D}_\beta, \quad (123)$$

with the covariant derivative \bar{D} and the local coupling to the phase field \mathbf{A}_\perp (see Eq. 98):

$$\bar{D} = \bar{\nabla} - ig \mathbf{A}_\perp(\bar{\mathbf{r}}) \quad g = \frac{3}{4\sqrt{2}} \sqrt{Re_L} \quad \mathbf{A}_\perp = \bar{\nabla} \phi(\bar{\mathbf{r}}), \quad (124)$$

Finally, the Dirac-adjoint wave function is used as a shortcut (see Eq. 114):

$$\bar{\psi}_\alpha(\bar{\mathbf{r}}) = \psi_\alpha^\dagger(\bar{\mathbf{r}}) i \gamma^0, \quad (125)$$

as well as the gamma matrices γ^β and the unit matrix \mathbf{I} in two dimensions (Eq. 113):

$$\gamma^0 = \begin{pmatrix} -i & 0 \\ 0 & i \end{pmatrix} \quad \gamma^1 = \begin{pmatrix} 0 & 1 \\ 1 & 0 \end{pmatrix} \quad \mathbf{I} = \begin{pmatrix} 1 & 0 \\ 0 & 1 \end{pmatrix}. \quad (126)$$

4.1.2 *Individual terms and interpretation* Expression Eq. 118 is separated into the following parts:

$$\mathcal{L} = \mathcal{L}_0^{laminar} + \mathcal{L}_0^{vortex} + \mathcal{L}' \quad (127)$$

$$\mathcal{L}_0^{laminar} = -\bar{\psi}_\alpha(\bar{\mathbf{r}}) \left(\mathbf{I}m_{eff.} + \hbar_{fl} \bar{\boldsymbol{\phi}} \right) \psi^\alpha(\bar{\mathbf{r}}) \quad (128)$$

$$\mathcal{L}_0^{vortex} = -\frac{1}{4} v^{-1} \mathbf{G}_{\alpha\beta}(\bar{\mathbf{r}}) \mathbf{G}^{\alpha\beta}(\bar{\mathbf{r}}) \quad (129)$$

$$\mathcal{L}' = iq \bar{\psi}_\alpha(\bar{\mathbf{r}}) \mathbf{A}_\perp(\bar{\mathbf{r}}) \psi^\alpha(\bar{\mathbf{r}}). \quad (130)$$

Where the fluid charge was defined as an auxiliary quantity:

$$q = \hbar_{fl} g. \quad (131)$$

The term $\mathcal{L}_0^{laminar}$ (Eq. 128) is rotation-free (see Section 3 in Part I) and is interpreted as a field of laminar flowing particles, with the particles referred to as “laminar (pseudo-)particles” or just “elementary laminars”.

\mathcal{L}_0^{vortex} (Eq. 129) forms a pure rotational field and is interpreted as a field of elementary vortices. \mathcal{L}' (Eq. 130) constitutes the coupling of the two fields. The individual terms, their properties and interpretation are considered in detail in the following paragraphs.

4.2 Properties of the fields and propagators

4.2.1 *Properties and propagator of the free laminar field* The Lagrangian density for elementary laminars Eq. 128 is examined in detail:

$$\mathcal{L}_0^{laminar} = -\bar{\psi}_\alpha(\bar{\mathbf{r}}) \left(\mathbf{I}m_{eff.} + \hbar_{fl} \bar{\boldsymbol{\phi}} \right) \psi^\alpha(\bar{\mathbf{r}}), \quad (132)$$

with the corresponding equation of motion (Euler-Lagrange formalism):

$$\left(\mathbf{I}m_{eff.} + \hbar_{fl} \bar{\boldsymbol{\phi}} \right) \psi^\alpha(\bar{\mathbf{r}}) = 0. \quad (133)$$

The solution approach is done in analogy to the solution of a Dirac equation. First, the kinematic momentum $\vec{\mathbf{p}} \in \mathbb{C}$ of a laminar particle, together with an inner product is needed:

$$\vec{\mathbf{p}} = ip^x + p^y \quad \text{with} \quad \vec{\mathbf{p}} \cdot \vec{\mathbf{q}} = \text{Re}(p^* q) = p^x q^x + p^y q^y. \quad (134)$$

Based on this, a two-momentum $\mathbf{p} \in \mathbb{C}^2$ is defined in analogy to the four-momentum of quantum electrodynamics according to:

$$\mathbf{p} = \begin{pmatrix} p^0 \\ p^1 \end{pmatrix} = \begin{pmatrix} \sqrt{m_{eff.}^2 + \vec{\mathbf{p}}^2} \\ ip^x + p^y \end{pmatrix}, \quad (135)$$

In addition to the kinematic momentum $\vec{\mathbf{p}}$, the two-momentum also contains m_{eff} as an auxiliary quantity, which is interpreted as the rest momentum.

For two two-vectors \mathbf{p}, \mathbf{q} according to definition Eq. 135, a Lorentzian inner product can be defined with (extended to \mathbb{C}^2 e.g. Friedman 2008):

$$\mathbf{p} \cdot \mathbf{q} = \text{Re}(g_{\alpha\beta} p^{*\alpha} q^\beta) = \frac{1}{2} g_{\alpha\beta} (p^{*\alpha} q^\beta + p^\alpha q^{*\beta}) \quad \alpha, \beta \in \{0, 1\}. \quad (136)$$

Where $g_{\alpha\beta} = \text{diag}(-1, +1)$ is used as seen in Par. 3.6.4. With this, the on shell condition holds as well:

$$\mathbf{p} \cdot \mathbf{p} = \text{Re}(-m_{eff}^2 - \vec{\mathbf{p}}^2 + \vec{\mathbf{p}}^2) = -m_{eff}^2. \quad (137)$$

Regarding the specific example, the two-momentum can be given in the rest frame of an undisturbed laminar particle, i.e. in the inertial frame traveling with the base flow. For the initial two-momentum \mathbf{p} as well as the final two-momentum \mathbf{p}' after scattering, it is valid that:

$$\mathbf{p} = \begin{pmatrix} m_{eff} \\ 0 \end{pmatrix} \quad \mathbf{p}' = \begin{pmatrix} \sqrt{m_{eff}^2 + (\vec{\mathbf{p}}')^2} \\ \vec{\mathbf{p}}' \end{pmatrix}. \quad (138)$$

By means of the two-momentum Eq. 135, two solution approaches for the equation of motion Eq. 133 with positive and negative frequency can be formulated respectively:

$$\psi^0(\vec{\mathbf{r}}) = \frac{1}{\sqrt{2p^0}} \mathbf{u}(\mathbf{p}) e^{i(\mathbf{p} \cdot \vec{\mathbf{r}})(\hbar_{fl} d_{box}^{SI})^{-1}} \quad \psi^1(\vec{\mathbf{r}}) = \frac{1}{\sqrt{2p^0}} \mathbf{v}(\mathbf{p}) e^{-i(\mathbf{p} \cdot \vec{\mathbf{r}})(\hbar_{fl} d_{box}^{SI})^{-1}}. \quad (139)$$

Whereby the scalar product Eq. 116 determines the periodicity of the exponent. Inserting ansatz Eq. 139 into Eq. 133 yields the equations of motion in momentum space:

$$(\mathbf{I}m_{eff} + i\mathcal{P}) \mathbf{u}(\mathbf{p}) = 0 \quad (\mathbf{I}m_{eff} - i\mathcal{P}) \mathbf{v}(\mathbf{p}) = 0. \quad (140)$$

For the normalization of the solutions of Eqs. 140 in momentum space it holds true that (Burgess & Moore, 2006):

$$\bar{\mathbf{u}}(\mathbf{p})\mathbf{u}(\mathbf{p}) = 2m_{eff} \quad \bar{\mathbf{v}}(\mathbf{p})\mathbf{v}(\mathbf{p}) = -2m_{eff}. \quad (141)$$

Therefore the following applies for the completeness relations (the additional spin sum is omitted in the two-dimensional case):

$$\mathbf{u}(\mathbf{p})\bar{\mathbf{u}}(\mathbf{p}) = \mathbf{I}m_{eff} - i\mathcal{P} \quad \mathbf{v}(\mathbf{p})\bar{\mathbf{v}}(\mathbf{p}) = -(\mathbf{I}m_{eff} + i\mathcal{P}). \quad (142)$$

From the one-particle solutions Eq. 139 of equation of motion Eq. 133, multi-particle solutions are constructed by linear combination:

$$\psi(\vec{\mathbf{r}}) = \int \frac{dp}{2\pi\sqrt{2p^0}} \left(a(\mathbf{p})\mathbf{u}(\mathbf{p}) e^{i(\mathbf{p} \cdot \vec{\mathbf{r}})(\hbar_{fl} d_{box}^{SI})^{-1}} + b^\dagger(\mathbf{p})\mathbf{v}(\mathbf{p}) e^{-i(\mathbf{p} \cdot \vec{\mathbf{r}})(\hbar_{fl} d_{box}^{SI})^{-1}} \right), \quad (143)$$

$$\bar{\psi}(\bar{\mathbf{r}}) = \int \frac{dp}{2\pi\sqrt{2p^0}} \left(a^\dagger(\mathbf{p})\bar{\mathbf{u}}(\mathbf{p})e^{-i(\mathbf{p}\cdot\bar{\mathbf{r}})(\hbar_{fl}d_{box}^{SI})^{-1}} + b(\mathbf{p})\bar{\mathbf{v}}(\mathbf{p})e^{i(\mathbf{p}\cdot\bar{\mathbf{r}})(\hbar_{fl}d_{box}^{SI})^{-1}} \right). \quad (144)$$

Where the amplitudes $a(\mathbf{p})$ and $b(\mathbf{p})$ are promoted to operators, satisfying the anticommutation relation:

$$\{a(\mathbf{p}), a^\dagger(\mathbf{p}')\} = 2\pi\delta(\mathbf{p} - \mathbf{p}') \quad \{b(\mathbf{p}), b^\dagger(\mathbf{p}')\} = 2\pi\delta(\mathbf{p} - \mathbf{p}'). \quad (145)$$

Consequently, the solution fields become operator-valued as well and form a quantum field:

$$\{\psi(\bar{\mathbf{r}}), \bar{\psi}(\bar{\mathbf{r}}')\} = \gamma^0\delta(\bar{\mathbf{r}} - \bar{\mathbf{r}}') \quad \{\psi(\bar{\mathbf{r}}), \psi(\bar{\mathbf{r}}')\} = 0. \quad (146)$$

Eventually, the propagator is needed for the scattering theory, which is given by:

$$S_F(\bar{\mathbf{r}}) = \lim_{\epsilon \rightarrow 0} \int \frac{d^2p}{(2\pi)^2} e^{i(\mathbf{p}\cdot\bar{\mathbf{r}})(\hbar_{fl}d_{box}^{SI})^{-1}} \frac{-i\not{\mathbf{p}} + \mathbf{I}m_{eff.}}{\mathbf{p}^2 + m_{eff.}^2 - i\epsilon}. \quad (147)$$

The latter forms the Green's function to the equation of motion of the free laminar field in position space (Eq. 133):

$$\left(\mathbf{I}m_{eff.} + \hbar_{fl}\vec{\not{\mathbf{D}}} \right) S_F(\bar{\mathbf{r}}) = \mathbf{I}\delta^2(\bar{\mathbf{r}}). \quad (148)$$

In momentum space, the propagator reads:

$$S_F(\mathbf{p}) = \frac{-i(-i\not{\mathbf{p}} + \mathbf{I}m_{eff.})}{\mathbf{p}^2 + m_{eff.}^2 - i\epsilon}. \quad (149)$$

The Feynman rules derived in this section are presented in Table 1.

4.2.2 Properties of the free vortex field The Lagrangian density of the vortex field is (Eq. 129):

$$\mathcal{L}_0^{vortex} = -\frac{1}{4}v^{-1}\mathbf{G}_{\alpha\beta}(\bar{\mathbf{r}})\mathbf{G}^{\alpha\beta}(\bar{\mathbf{r}}). \quad (150)$$

For the ansatz, in analogy to Eq. 135 based on the wave vector $\vec{\mathbf{k}}$, a two-wave vector is defined as an auxiliary quantity:

$$\mathbf{k} = \begin{pmatrix} k \\ \vec{\mathbf{k}} \end{pmatrix} \quad \mathbf{k}' = \begin{pmatrix} k' \\ \vec{\mathbf{k}}' \end{pmatrix}, \quad (151)$$

where $k = |\vec{\mathbf{k}}|$ is the magnitude of the wave vector. \mathbf{k} denotes the two-wave vector before and \mathbf{k}' after scattering, again applied to the specific example. For the two-wave vector, using Eq. 136, the on shell condition reads:

Feynman rules for laminars		
incoming laminar		$u(\mathbf{p})$
outgoing laminar		$\bar{u}(\mathbf{p})$
laminar propagator		$\frac{-i(-i\not{p} + \mathbf{I}m_{eff.})}{\mathbf{p}^2 + m_{eff.}^2 - i\epsilon}$

Table 1: Feynman rules in momentum space for elementary laminar pseudo-particles.

$$\mathbf{k}^2 = (\mathbf{k}')^2 = 0. \quad (152)$$

Since Eq. 150 is defined with respect to a finite box, the vortex field can be quantized and takes the following form as an operator field:

$$\mathbf{A}(\mathbf{r}) = \int \frac{dk}{2\pi\sqrt{2\omega}} \left(a(\mathbf{k})\boldsymbol{\varepsilon}(\mathbf{k})e^{i\mathbf{k}\cdot\bar{\mathbf{r}}/d_{box}^{SI}} + a^\dagger(\mathbf{k})\boldsymbol{\varepsilon}^\dagger(\mathbf{k})e^{-i\mathbf{k}\cdot\bar{\mathbf{r}}/d_{box}^{SI}} \right), \quad (153)$$

in which the angular frequency $\omega = v|\mathbf{k}|$ was used. The amplitudes $a(\mathbf{k})$ are regarded as operators satisfying the commutation relation:

$$[a(\mathbf{k}), a^\dagger(\mathbf{k}')] = 2\pi\delta(\mathbf{k} - \mathbf{k}'). \quad (154)$$

In two dimensions there is only one polarization direction $\boldsymbol{\varepsilon}(\mathbf{k})$, so the additional summation over the polarizations is omitted. Therefore, the following normalization is valid:

$$\varepsilon_\alpha^*(\mathbf{k})\varepsilon^\alpha(\mathbf{k}) = 1, \quad (155)$$

as well as the completeness relation (polarization sum):

$$\varepsilon_\alpha(\mathbf{k})\varepsilon_\beta^*(\mathbf{k}) = g_{\alpha\beta} \quad \text{as well as} \quad \varepsilon^\alpha(\mathbf{k})\varepsilon_\beta^*(\mathbf{k}) = g_\beta^\alpha = \delta_\beta^\alpha. \quad (156)$$

Finally, the Hamiltonian of vortex quasiparticles Eq. 150 can be expressed as:

$$\begin{aligned} H_0^{vortex} &= v^{-1} \int \frac{dk}{2\pi\sqrt{2\omega}} \hbar_{fl}\omega \left(a^\dagger(\mathbf{k})a(\mathbf{k}) + \frac{1}{2} \right) \\ &= \int \frac{dk}{2\pi\sqrt{2\omega}} \hbar_{fl}k \left(a^\dagger(\mathbf{k})a(\mathbf{k}) + \frac{1}{2} \right), \end{aligned} \quad (157)$$



Feynman rules for vortices		
incoming vortex		$\varepsilon_\alpha(\mathbf{k})$
outgoing vortex		$\varepsilon_\alpha^*(\mathbf{k})$

Table 2: Feynman rules in momentum space for elementary vortex pseudo-particles.

which corresponds to the momentum density of single quanta with momentum magnitude given by:

$$p^{vortex} = \hbar_{fl} k. \quad (158)$$

The Feynman rules derived in this section are presented in Table 2.

Remark 9 (Transformation properties under time inversion) *Due to the definition of the time axis parallel to the base flow direction, it is possible that the elementary vortices move in reversed time direction after the scattering process. This happens in the rest frame of the elementary laminar if the scattering angle $\theta > \pi/2$ (Fig. 6). The behavior of the vortex field under time inversion is briefly investigated in order to estimate the effect on the effective cross section later.*

Since the polarization ε is to be preserved under time inversion $\bar{x}_0^M = vt \rightarrow -vt$, the second coordinate \bar{x}_1^M must be inverted, because $\text{sgn}(\varepsilon) = \text{sgn}(\bar{\mathbf{x}}_0^M \times \bar{\mathbf{x}}_1^M)$. This is possible due to the axial symmetry of the scattering cross section around the \bar{x}_0^M axis, whereby the substitution $\bar{x}_1^M \rightarrow -\bar{x}_1^M$ leaves the scattering cross section invariant.

The creation and annihilation operators Eq. 154 remain constant under time inversion due to the symmetry of the delta distribution $\delta(-x) = \delta(x)$, which allows the time-inverted vortex field $\check{\mathbf{A}}$ to be given as:

$$\check{\mathbf{A}}(\mathbf{r}) = \int \frac{dk}{2\pi\sqrt{2\omega}} \left(a(\mathbf{k})\varepsilon(\mathbf{k})e^{-i\mathbf{k}\cdot\bar{\mathbf{r}}/d_{box}^{SI}} + a^\dagger(\mathbf{k})\varepsilon^\dagger(\mathbf{k})e^{i\mathbf{k}\cdot\bar{\mathbf{r}}/d_{box}^{SI}} \right). \quad (159)$$

I.e. time inversion swaps the signs of the exponents. On the other hand, field $\check{\mathbf{A}}$ in Eq. 159 is equal to the original vortex field \mathbf{A} (Eq. 153) with inverted sign of the metric tensor $g_{\alpha\beta} \rightarrow -g_{\alpha\beta} = \check{g}_{\alpha\beta}$ (Burgess & Moore, 2006).

Therefore, if the elementary vortex in the scattering process reverses the direction of motion with respect to the time axis, this can be mapped by using the time-inverted completeness relation for the outgoing elementary vortex:

$$\check{\varepsilon}_\alpha(\mathbf{k})\check{\varepsilon}_\beta^*(\mathbf{k}) = \check{g}_{\alpha\beta} = -g_{\alpha\beta} \quad \text{as well as} \quad \check{\varepsilon}^\alpha(\mathbf{k})\check{\varepsilon}_\beta^*(\mathbf{k}) = g^{\alpha\gamma}\check{g}_{\gamma\beta} = -\delta_\beta^\alpha. \quad (160)$$

Feynman rules for vertices

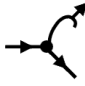
vertex laminar-vortex-laminar  $q\gamma^\beta$

Table 3: Feynman rule in momentum space for vertices.

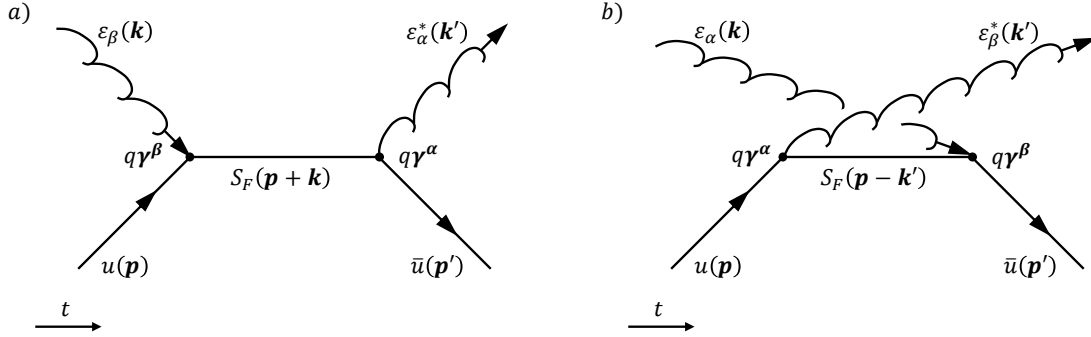


Figure 5: First-order Feynman diagrams contributing to the invariant matrix element $\mathcal{M} = \mathcal{M}_1 + \mathcal{M}_2$ of the scattering of an elementary vortex by a laminar particle. a) shows the contribution \mathcal{M}_1 , b) the contribution \mathcal{M}_2 .

4.2.3 Vertices The interaction Lagrangian density \mathcal{L}' (Eq. 130) forms the minimum coupling of the laminar and vortex fields:

$$\mathcal{L}' = iq\bar{\psi}_\alpha(\bar{\mathbf{r}})\gamma^\beta \mathbf{A}_\beta^\perp(\bar{\mathbf{r}})\psi^\alpha(\bar{\mathbf{r}}). \quad (161)$$

In momentum space, the contribution of the interaction term becomes:

$$\mathbf{j}^\beta = q\gamma^\beta, \quad (162)$$

with the fluid charge q according to definition Eq. 131. The derived Feynman rule for vertices is shown in Table 3.

4.3 Scattering amplitude/ invariant matrix element \mathcal{M}

4.3.1 Relevant Feynman diagrams The two-particle scattering process of an elementary vortex with an elementary laminar particle in first order perturbation theory is considered. The corresponding Feynman diagrams are shown in Fig. 5.

These diagrams build the two-dimensional fluid equivalent of Compton scattering, which serves as the template for this process.

4.3.2 Insertion into the invariant matrix element \mathcal{M} The scattering amplitude, expressed as an invariant matrix element \mathcal{M} , is composed of the contributions of the two Feynman graphs in Fig. 5:

$$\mathcal{M} = \mathcal{M}_1 + \mathcal{M}_2. \quad (163)$$

The individual contributions are combined according to the definitions in Par. 4.2 and are given in momentum space by:

$$i\mathcal{M}_1 = -iq^2 \varepsilon_\alpha^*(\mathbf{k}') \varepsilon_\beta(\mathbf{k}) \bar{\mathbf{u}}(\mathbf{p}') \frac{\gamma^\alpha (-i\not{\mathbf{p}} - i\hbar_{fl}\not{\mathbf{k}} + \mathbf{I}m_{eff.}) \gamma^\beta}{(\mathbf{p} + \hbar_{fl}\mathbf{k})^2 + m_{eff.}^2} \mathbf{u}(\mathbf{p}), \quad (164)$$

$$i\mathcal{M}_2 = -iq^2 \varepsilon_\beta^*(\mathbf{k}') \varepsilon_\alpha(\mathbf{k}) \bar{\mathbf{u}}(\mathbf{p}') \frac{\gamma^\beta (-i\not{\mathbf{p}} + i\hbar_{fl}\not{\mathbf{k}}' + \mathbf{I}m_{eff.}) \gamma^\alpha}{(\mathbf{p} - \hbar_{fl}\mathbf{k}')^2 + m_{eff.}^2} \mathbf{u}(\mathbf{p}). \quad (165)$$

4.4 Auxiliary quantities

For the calculation of an effective cross section from the invariant matrix elements Eqs. 164 and 165, a few additional relations from scattering theory are needed. These are briefly introduced in this paragraph and adapted to the two-dimensional fluid case.

4.4.1 Mandelstam variables and deductions Mandelstam variables are defined for general two-body to two-body scattering processes and are independent of the exact configuration. For the scattering process of a laminar particle with two-momentum \mathbf{p} before the scattering process and \mathbf{p}' thereafter, and an elementary vortex with two-wave vector \mathbf{k} before and \mathbf{k}' afterwards, the Mandelstam variables are calculated as follows (Burgess & Moore, 2006):

$$\begin{aligned} s &= -(\mathbf{p} + \hbar_{fl}\mathbf{k})^2 = -(\mathbf{p}' + \hbar_{fl}\mathbf{k}')^2 \\ t &= -(\mathbf{p} - \mathbf{p}')^2 = -(\hbar_{fl}\mathbf{k}' - \hbar_{fl}\mathbf{k})^2 \\ u &= -(\mathbf{p} - \hbar_{fl}\mathbf{k}')^2 = -(\mathbf{p}' - \hbar_{fl}\mathbf{k})^2. \end{aligned} \quad (166)$$

One implements the already defined two-momenta \mathbf{p} and \mathbf{p}' from Eq. 138 and the two-wave vectors \mathbf{k} and \mathbf{k}' from Eq. 151 and obtains for the studied scattering process in the rest frame of the laminar particle:

$$\begin{aligned} s &= -2\hbar_{fl}(\mathbf{p} \cdot \mathbf{k}) + m_{eff.}^2 = -2\hbar_{fl}(\mathbf{p}' \cdot \mathbf{k}') + m_{eff.}^2 = 2m_{eff.}\hbar_{fl}k + m_{eff.}^2 \\ t &= 2(\mathbf{p} \cdot \mathbf{p}') + 2m_{eff.}^2 = 2\hbar_{fl}^2(\mathbf{k} \cdot \mathbf{k}') = 2\hbar_{fl}^2 kk'(\cos\theta - 1) \\ u &= 2\hbar_{fl}(\mathbf{p}' \cdot \mathbf{k}) + m_{eff.}^2 = 2\hbar_{fl}(\mathbf{p} \cdot \mathbf{k}') + m_{eff.}^2 = -2m_{eff.}\hbar_{fl}k' + m_{eff.}^2. \end{aligned} \quad (167)$$

The geometry and scattering angle θ in the rest frame of the laminar particle (lab-frame) are defined according to Fig. 6. In general, the following relation also holds for the Mandelstam variables:

$$s + t + u = 2m_{eff.}^2, \quad (168)$$

with which further relations can be derived in the rest frame of the laminar particle:

$$\frac{1}{k} - \frac{1}{k'} = \frac{\hbar_{fl}}{m_{eff.}}(\cos\theta - 1), \quad (169)$$

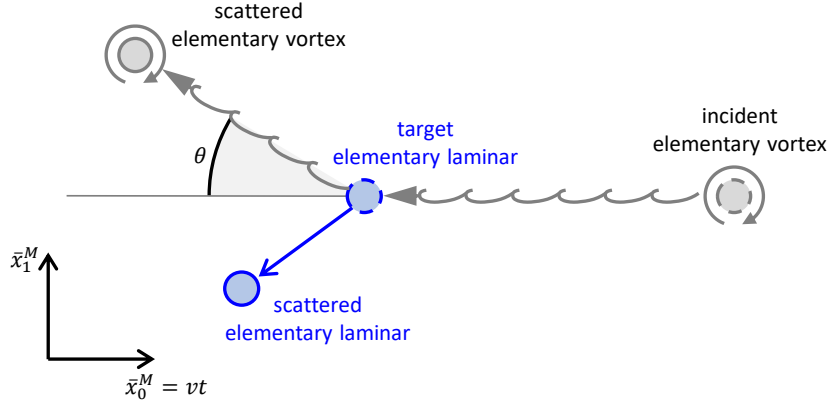


Figure 6: Definition of the scattering angle θ in the rest frame of the laminar particle. The resting laminar particle (dashed blue) is hit by an incoming elementary vortex from the right against time direction (dashed gray). The angle between the incoming and outgoing elementary vortices (gray) is defined as the scattering angle θ . For $\theta > \pi/2$ the outgoing elementary vortex travels with the time direction.

$$\frac{dt}{d(\cos \theta)} = 2(\hbar_{fl} k')^2. \quad (170)$$

From Eq. 169, the ratio P between the vortex wavenumbers after and before the collision can be determined:

$$P(k, x_0^M, \theta) = \frac{k'}{k} = \frac{1}{1 - \frac{\hbar_{fl} k}{m_{eff}} (\cos \theta - 1)}, \quad (171)$$

resulting in the momentum transfer Δp during the impact:

$$\Delta p(k, x_0^M, \theta) = \hbar_{fl} \Delta k = \hbar_{fl} (k - k') = \hbar_{fl} k \left(1 - P(k, x_0^M, \theta)\right). \quad (172)$$

4.4.2 trace techniques The matrices $\{\gamma^j\}$ as specified in Eq. 126 are part of the Clifford algebra $Cl(2, 0)$ and form a basis of the subspace $Cl^1(2, 0)$ resp. $Cl^1(2)$ in the analytic continuation. This property defines their behavior under permutation of the individual terms in the evaluation of path integrals. The defining property reads (see also Eq. 13):

$$\gamma^\alpha \gamma^\beta + \gamma^\beta \gamma^\alpha = 2g^{\alpha\beta} \mathbf{I} \quad \alpha, \beta = 0, 1. \quad (173)$$

With the metric tensor $g^{\alpha\beta} = \text{diag}(-1, +1)$ (see Par. 3.6.4). The contractions needed for evaluation are as follows in the two-dimensional case:

$$\gamma^\alpha \gamma_\alpha = 2\mathbf{I} \quad \text{Tr}(\gamma^\alpha \gamma_\alpha) = 4. \quad (174)$$

The trace of the product of two gamma matrices can be determined by cyclic permutation:

$$\text{Tr}(\gamma^\alpha \gamma^\beta) = \text{Tr}\left(\frac{1}{2} \gamma^\alpha \gamma^\beta + \frac{1}{2} \gamma^\beta \gamma^\alpha\right) = g^{\alpha\beta} \text{Tr}(\mathbf{I}) = 2g^{\alpha\beta}, \quad (175)$$

which for slashed quantities ($\not{a} = \gamma^\alpha a_\alpha$, see Eq. 123) means that:

$$\begin{aligned} \text{Tr}(\text{Re}(\not{a}\not{b})) &= \text{Tr}(\gamma^\alpha \gamma^\beta \text{Re}(a_\alpha^* b_\beta)) \\ &= 2g^{\alpha\beta} \text{Re}(a_\alpha^* b_\beta) = 2(\mathbf{a} \cdot \mathbf{b}). \end{aligned} \quad (176)$$

In the last step the scalar product Eq. 136 was used. Finally, the following contraction is required:

$$\gamma^\alpha \gamma^\nu \gamma_\alpha = (2g^{\alpha\nu} \mathbf{I} - \gamma^\nu \gamma^\alpha) \gamma_\alpha = 2\gamma^\nu \mathbf{I} - 2\gamma^\nu \mathbf{I} = 0. \quad (177)$$

Remark 10 *This contraction Eq. 177 is different in the two-dimensional compared to the four-dimensional case, where $\gamma^\nu \gamma^\alpha \gamma_\nu = -2\gamma^\alpha$, since there the summation is done over 4 generators. This difference simplifies the calculation of the cross section considerably compared to the four-dimensional case, because contributions of higher order disappear.*

For terms with an odd number of γ -matrices, it holds, as in the four-dimensional case, that:

$$\text{Tr}(\gamma^\alpha) = \text{Tr}(\gamma^\alpha \gamma^\beta \gamma^\delta) = \dots = 0. \quad (178)$$

4.5 Invariant matrix element squared, mixing terms

The squared unpolarized invariant matrix element $\overline{|\mathcal{M}|^2}$ is calculated, which contains the sum over all possible spin and polarization states s and p :

$$\overline{|\mathcal{M}|^2} = \sum_{s,p,s',p'} |\mathcal{M}|^2. \quad (179)$$

Based on the symmetries of the matrix elements of the individual Feynman diagrams Eqs. 164 and 165, the squared unpolarized matrix element is calculated as:

$$\overline{|\mathcal{M}|^2} = (\overline{\mathcal{M}}_1 + \overline{\mathcal{M}}_2) (\overline{\mathcal{M}}_1 + \overline{\mathcal{M}}_2)^\dagger = \overline{|\mathcal{M}}_1|^2 + \overline{|\mathcal{M}}_2|^2 + 2\text{Re}(\overline{\mathcal{M}}_1 \overline{\mathcal{M}}_2^\dagger). \quad (180)$$

The expressions can be evaluated separately. First, $\overline{|\mathcal{M}}_1|^2$ is considered. The corresponding polarized matrix element is (using cyclic permutation in the trace, as well as on-shell conditions Eqs. 137 and 152 to simplify the denominator):

$$\begin{aligned} |\mathcal{M}_1|^2 &= q^4 \text{Tr} \left[\varepsilon^\delta(\mathbf{k}') \varepsilon_\alpha^*(\mathbf{k}') \varepsilon^{*\zeta}(\mathbf{k}) \varepsilon_\beta(\mathbf{k}) \mathbf{u}(\mathbf{p}') \bar{\mathbf{u}}(\mathbf{p}') \frac{\gamma^\alpha (i\not{p} + i\hbar_{fl} \not{k} - \mathbf{I}m_{eff.}) \gamma^\beta}{2\hbar_{fl}(\mathbf{p} \cdot \mathbf{k})} \right. \\ &\quad \left. \times \mathbf{u}(\mathbf{p}) \bar{\mathbf{u}}(\mathbf{p}) \frac{\gamma_\zeta (i\not{p} + i\hbar_{fl} \not{k} - \mathbf{I}m_{eff.}) \gamma_\delta}{2\hbar_{fl}(\mathbf{p} \cdot \mathbf{k})} \right]. \end{aligned} \quad (181)$$

In the transition to the unpolarized matrix element, the polarization and spin sums allow the completeness relations 142 and 156 to be applied (the step is purely formal in two dimensions, since in each case the summation is over a single spin and polarization state):

$$\begin{aligned} \overline{|\mathcal{M}_1|^2} &= \frac{q^4}{4\hbar_{fl}^2(\mathbf{p} \cdot \mathbf{k})^2} \text{Tr} \left[\gamma_\alpha(-i\boldsymbol{\psi}' + \mathbf{I}m_{eff.})\gamma^\alpha(i\boldsymbol{\psi} + i\hbar_{fl}\boldsymbol{k} - \mathbf{I}m_{eff.}) \right. \\ &\quad \left. \times \gamma^\beta(-i\boldsymbol{\psi} + \mathbf{I}m_{eff.})\gamma_\beta(i\boldsymbol{\psi} + i\hbar_{fl}\boldsymbol{k} - \mathbf{I}m_{eff.}) \right]. \end{aligned} \quad (182)$$

To evaluate the gamma matrices outside the brackets γ^α and γ^β , relations Eqs. 174 and 177 are used. This simplifies the equation significantly in the two-dimensional case because of Remark 10:

$$\begin{aligned} \overline{|\mathcal{M}_1|^2} &= \frac{q^4}{4\hbar_{fl}^2(\mathbf{p} \cdot \mathbf{k})^2} \text{Tr} \left[2\mathbf{I}m_{eff.}(i\boldsymbol{\psi} + i\hbar_{fl}\boldsymbol{k} - \mathbf{I}m_{eff.}) \right. \\ &\quad \left. \times 2\mathbf{I}m_{eff.}(i\boldsymbol{\psi} + i\hbar_{fl}\boldsymbol{k} - \mathbf{I}m_{eff.}) \right]. \end{aligned} \quad (183)$$

The remainder is expanded and the trace is evaluated using relations Eqs. 174, 176 and again on shell conditions Eqs. 137 and 152:

$$\begin{aligned} \overline{|\mathcal{M}_1|^2} &= \frac{q^4}{4\hbar_{fl}^2(\mathbf{p} \cdot \mathbf{k})^2} \left[16m_{eff.}^4 - 16m_{eff.}^2\hbar_{fl}(\mathbf{p} \cdot \mathbf{k}) - 8m_{eff.}^2\hbar_{fl}^2(\mathbf{k} \cdot \mathbf{k}) \right] \\ &= \frac{q^4}{\hbar_{fl}^2(\mathbf{p} \cdot \mathbf{k})^2} \left[4m_{eff.}^4 - 4m_{eff.}^2\hbar_{fl}(\mathbf{p} \cdot \mathbf{k}) \right]. \end{aligned} \quad (184)$$

Finally, the scalar products are evaluated by inserting the relations from Eq. 167:

$$\overline{|\mathcal{M}_1|^2} = \frac{q^4}{(m_{eff.}\hbar_{fl}k)^2} \left[4m_{eff.}^4 + 4m_{eff.}^3\hbar_{fl}k \right]. \quad (185)$$

The same principles can be applied to calculate the mixed element $\overline{\mathcal{M}_1\mathcal{M}_2^\dagger}$:

$$\begin{aligned} \overline{\mathcal{M}_1\mathcal{M}_2^\dagger} &= \frac{q^4}{4\hbar_{fl}^2(\mathbf{p} \cdot \mathbf{k})(-\mathbf{p}' \cdot \mathbf{k})} \text{Tr} \left[\gamma_\alpha(-i\boldsymbol{\psi}' + \mathbf{I}m_{eff.})\gamma^\alpha(i\boldsymbol{\psi} + i\hbar_{fl}\boldsymbol{k} - \mathbf{I}m_{eff.}) \right. \\ &\quad \left. \times \gamma^\beta(-i\boldsymbol{\psi} + \mathbf{I}m_{eff.})\gamma_\beta(i\boldsymbol{\psi} - \hbar_{fl}i\boldsymbol{k}' - \mathbf{I}m_{eff.}) \right]. \end{aligned} \quad (186)$$

Evaluation of γ^α and γ^β :

$$\begin{aligned} \overline{\mathcal{M}_1\mathcal{M}_2^\dagger} &= \frac{-q^4}{4\hbar_{fl}^2(\mathbf{p} \cdot \mathbf{k})(\mathbf{p}' \cdot \mathbf{k})} \text{Tr} \left[2\mathbf{I}m_{eff.}(i\boldsymbol{\psi} + i\hbar_{fl}\boldsymbol{k} - \mathbf{I}m_{eff.}) \right. \\ &\quad \left. \times 2\mathbf{I}m_{eff.}(i\boldsymbol{\psi} - i\hbar_{fl}\boldsymbol{k}' - \mathbf{I}m_{eff.}) \right]. \end{aligned} \quad (187)$$

Expand and evaluate the trace:

$$\overline{\mathcal{M}_1 \mathcal{M}_2^\dagger} = \frac{-q^4}{4\hbar_{fl}^2(\mathbf{p} \cdot \mathbf{k})(\mathbf{p}' \cdot \mathbf{k})} \left[16m_{eff}^4 - 8m_{eff}^2 \hbar_{fl}(\mathbf{k} \cdot \mathbf{p}) + 8m_{eff}^2 \hbar_{fl}(\mathbf{k}' \cdot \mathbf{p}) + 8m_{eff}^2 \hbar_{fl}^2(\mathbf{k} \cdot \mathbf{k}') \right]. \quad (188)$$

Compute the scalar products with the help of relations Eq. 167:

$$\overline{\mathcal{M}_1 \mathcal{M}_2^\dagger} = \frac{-q^4}{m_{eff}^2 \hbar_{fl}^2 k k'} \left[4m_{eff}^4 + 2m_{eff}^3 \hbar_{fl} k - 2m_{eff}^3 \hbar_{fl} k' + 2m_{eff}^2 \hbar_{fl}^2 k k' (\cos \theta - 1) \right]. \quad (189)$$

Due to the symmetries presented in Par. 4.4.1, the matrix element $\overline{|\mathcal{M}_2|^2}$ can be determined directly from $\overline{|\mathcal{M}_1|^2}$ by performing a substitution $k \rightarrow -k'$:

$$\overline{|\mathcal{M}_2|^2} = \frac{q^4}{(m_{eff} \hbar_{fl} k')^2} \left[4m_{eff}^4 - 4m_{eff}^3 \hbar_{fl} k' \right]. \quad (190)$$

To obtain the squared unpolarized invariant matrix element $\overline{|\mathcal{M}|^2}$, Eqs. 185, 189 and 190 are substituted into Eq. 180. This expression is simplified using relation Eq. 169, and the following result is obtained:

$$\overline{|\mathcal{M}|^2} = 4q^4 (\cos^2 \theta - \cos \theta). \quad (191)$$

4.6 Differential cross section

The cross section per momentum transfer for the two-particle scattering process is calculated as a function of the invariant matrix element using (e.g. Chiochia, Dissertori & Gehrmann 2010):

$$\frac{d\sigma}{dt} = \frac{1}{16\pi(s - m^2)^2} \overline{|\mathcal{M}|^2} = \frac{1}{16\pi(2m_{eff} \hbar_{fl} k)^2} \overline{|\mathcal{M}|^2}. \quad (192)$$

Where in the last step relation Eq. 167 was used. By means of Eq. 170 the angular dependence of the differential cross section can be determined, and inserting matrix element Eq. 191, one obtains:

$$\frac{d\sigma(k, x_0^M, \theta)}{d(\cos \theta)} = \frac{2(\hbar_{fl} k')^2}{16\pi(2m_{eff} \hbar_{fl} k)^2} \overline{|\mathcal{M}|^2} = \frac{q^4}{8\pi m_{eff}^2} \left(\frac{k'}{k} \right)^2 (\cos^2 \theta - \cos \theta). \quad (193)$$

With aid of Eq. 171, the differential cross section can be expressed as a function of ratio P and with respect to the solid angle element $d\Omega = -d(\cos \theta)$:

$$-\frac{d\sigma(k, x_0^M, \theta)}{d(\cos \theta)} = \frac{d\sigma(k, x_0^M, \theta)}{d\Omega} = \frac{q^4}{8\pi m_{eff}^2} P^2(k, x_0^M, \theta) (\cos \theta - \cos^2 \theta). \quad (194)$$

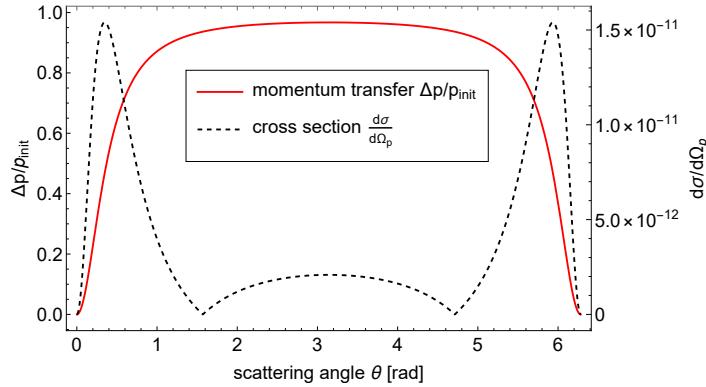


Figure 7: Dependency of the differential cross section and momentum transfer from scattering angle θ . Exemplary representation for numerical values as in the flight example (Table 5), evaluated at position $k = 250$ and $x_1 = 0.6$.

However, cross section Eq. 194 becomes negative for scattering angles $\theta > \pi/2$. One recalls in this regard Remark 9, which states that in this case the time-inverted polarization sum for the outgoing elementary vortex Eq. 160 is to be used. This in turn reverses the sign of the squared unpolarized matrix elements Eqs. 181 & 186 and therefore of the cross section for $\theta > \pi/2$. The cross section including the effect of time inversion can thus be given as:

$$\frac{d\sigma(k, x_0^M, \theta)}{d\Omega} = \frac{q^4}{8\pi m_{eff}^2} P^2(k, x_0^M, \theta) |\cos \theta - \cos^2 \theta|. \quad (195)$$

The differential cross section Eq. 195 is shown in Fig. 7.

Remark 11 *Due to the fact that both \hbar_{fl} (Eq. 119) and m_{eff} (Eq. 120) depend on the value of coordinate x_0^M , the cross section Eq. 195 is a function of the position x_0^M in flow direction. This is not a problem as long as the dependency is sufficiently weak such that the cross section can be assumed to be approximately constant over a box (see Par. 3.5).*

5 Model and results

In this section, a model for the formation of TS waves is created by applying the proposed theory, and results are calculated for a specific example.

The idea of the model is that there are both elementary laminar and vortex particles according to Section 4 in the flow above the plate. These particles scatter among themselves. In the process of scattering, the wavenumbers of elementary vortices can be lowered and their rotation is gradually slowed down by repeated collisions. Since the effect is stronger for elementary vortices with high wavenumbers, the wavenumbers and thus the frequencies of individual vortices become more and more equal. The resulting resonance in the occupation number of elementary vortices with certain frequencies is

then interpreted classically as an amplification of these frequencies and is identified with the amplification factor n from e^N -theory.

The model considers only scattering events along a profile of constant velocity and with maximum amount of wavenumber transferred. Therefore, the first two modeling steps consist of finding the height in the velocity profile (Par. 5.1) and the local scattering angle (Par. 5.2) including the most scattering events with the largest transfer of wavenumber.

Taking into account the surroundings of the particles in Par. 5.3, the probability of wavenumber transmission per collision is estimated, which is then used to calculate the change in occupation number – and consequently the amplification – of different frequencies in Par. 5.4.

As a result, an analytical expression for the maximum amplification factor $N(x_1)$ as a function of position x_1 is derived, together with an approximate formula for the transition point $x_{trans.}^{Sc}$ at which the maximum amplification factor exceeds a fixed value (e.g. $N = 9$) in Par. 5.5. The model is computed exemplarily with numerical values corresponding to the introductory examples (Fig. 2).

Nomenclature: In order to achieve conformity with fluid mechanical literature, the notation in Euclidean space is applied with the value of the dimensionless coordinate x_1 in the direction of the flow. Since only scalar quantities at fixed times are used, the transformation from Minkowski to Euclidean space is straightforward with a substitution $x_0^M \rightarrow x_1$.

5.1 Estimating the distribution of elementary vortices in the boundary layer

5.1.1 Plate front as a source of elementary vortices Since the scattering theory is formulated for a thin layer with constant flow velocity only, the height h in the velocity profile of the boundary layer is sought at which the maximum amount of scattering events can be expected. Because both a laminar particle and an elementary vortex are required as input quantities for a scattering process, most events will occur where both types of particles are mixed. Consequently, a practical consideration for the distribution of elementary vortices and laminar particles in the boundary layer is needed.

In the model, the front of the plate at coordinate origin is taken as a point source for elementary vortices. This is equivalent to the assumption that laminar particles from the free flow hit the front with an average velocity v_∞^{SI} (see also Fig. 1), and their momentum is converted virtually completely into angular momentum. After formation, the resulting elementary vortices are positioned near the plate surface and move into the boundary layer by diffusion or residual momentum.

Therefore, only elementary vortices are present directly above the plate surface, and their concentration decreases with increasing distance η from the plate, while the undisturbed volume flux – consisting of laminar particles – increases with distance from the surface (Fig. 8a).

Transferred to the continuous model of the boundary layer, the elementary vortices

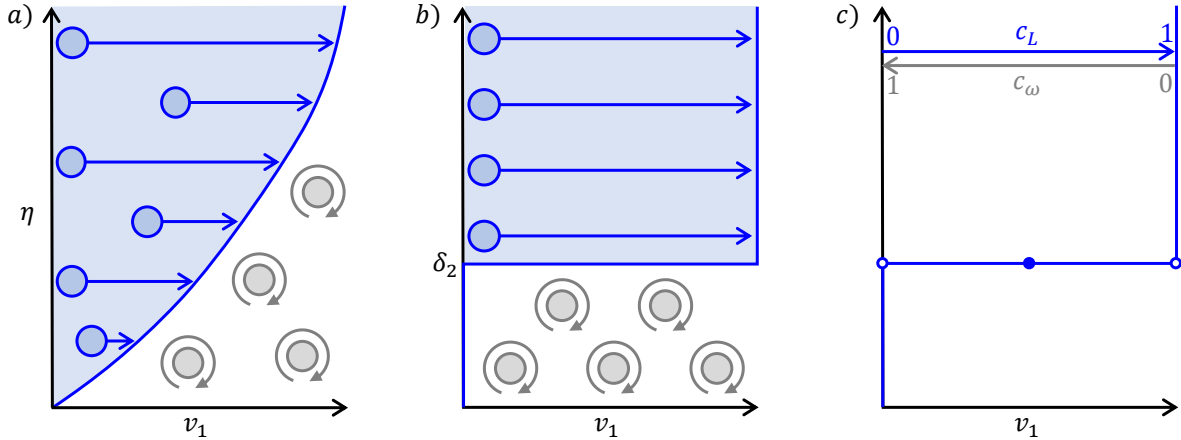


Figure 8: a) Schematic representation of the distribution of laminar particles and elementary vortices in the boundary layer. In reality, mixed particles with a wide range of momentum and angular momentum are to be expected. b) Model assumption: The particles occur in an ordered fashion and as pure laminars or vortices. Since the laminar particles contain all the momentum, their lower limit corresponds to the momentum thickness δ_2 . c) Transfer of this situation to the concentrations/ amount fractions of laminar and vortex particles c_L and c_ω (indicated with separate scales). These take the form of Heaviside step functions.

form the velocity defect caused by the plate. The local flow velocity thus becomes a measure of the respective proportions of laminar and vortex particles, which can be expressed as amount fractions c_L and c_ω . For ideal collision conditions, one searches for the height in the profile at which the amount fractions of laminar and vortex particles are equal:

$$c_L = c_\omega = 0.5. \quad (196)$$

5.1.2 Simplification as Heaviside step function The simplification is achieved by assuming that the transition from vortical to laminar particles with increasing height in the profile is not continuous, but approximated as a Heaviside step function at height h (Fig. 8b), with the amount fractions c_L and c_ω as a function of the profile height x_2^{SI} (schematically shown in Fig. 8c):

$$c_L(x_2^{SI}) = \begin{cases} 1 & x_2^{SI} > h \\ 0.5 & x_2^{SI} = h \\ 0 & x_2^{SI} < h \end{cases} \quad c_\omega(x_2^{SI}) = \begin{cases} 0 & x_2^{SI} > h \\ 0.5 & x_2^{SI} = h \\ 1 & x_2^{SI} < h \end{cases} \quad (197)$$

In this simplified situation, condition Eq. 196 is satisfied at the height of the step h and all scattering events take place at this height.

5.1.3 Determination of h According to the model assumption, only the laminar particles possess momentum, while the vortex particles are equipped solely with angular

momentum. Therefore, in the approximation with the Heaviside velocity profile according to Par. 5.1.2, the total momentum flux is found above height h .

Since this flow is composed of laminar particles alone, it is an undisturbed flow with h as the lower edge (Fig. 8b), which in fact corresponds to the definition of momentum thickness δ_2 (see e.g. Schlichting & Gersten 2017). Thus, height h of the step can be equated with the momentum thickness δ_2 , which in the initial laminar boundary layer is given by:

$$h = \delta_2 = 0.664 \sqrt{\frac{\mu^{SI} x_1^{SI}}{\rho^{SI} v_\infty^{SI}}}. \quad (198)$$

The scattering theory is therefore applied at height of the momentum thickness δ_2 Eq. 198 (red dashed line in Figs. 1 and 4). As required, the dimensionless velocity v relevant for the scattering theory is constant at this height and given by:

$$v = \frac{v^{SI}}{v_\infty^{SI}} = 0.664 \cdot c_1 = 0.664 \cdot 0.332 = 0.220. \quad (199)$$

5.2 Simplification: Scattering angle with maximum wavenumber transfer

The different types of particles in the boundary layer scatter among themselves, with first-order processes according to Feynman graphs Fig. 5 describing the scattering process between a laminar and a vortex particle. In this process, the wavenumber $k = |\mathbf{k}|$ of the elementary vortex decreases during the collision (analogous to Compton scattering in quantum mechanics).

A simplification is achieved by considering only those scattering events with maximum wavenumber transfer Δk . The angular dependency of wavenumber transfer is given by (according to Eq. 172):

$$\Delta k(k, x_1, \theta) = \frac{\Delta p(k, x_1, \theta)}{\hbar_{fl}} = k \left(1 - P(k, x_1, \theta) \right), \quad (200)$$

as a function of the wavenumber ratio P after and before scattering according to Eq. 171. The wavenumber transfer is illustrated in Fig. 7. The largest transmission occurs at a scattering angle of 180° and it is set:

$$\theta_{max} = \pi. \quad (201)$$

One obtains the maximum quantities by substituting angle Eq. 201 into the respective definitions. The ratio $P_{\theta_{max}}$ at maximum scattering angle (from Eq. 171) is given by:

$$P_{\theta_{max}}(k, x_1) = P(k, x_1, \theta_{max}) = \left(1 + \frac{2\hbar_{fl}k}{m_{eff.}} \right)^{-1}. \quad (202)$$

From that, the maximum wavenumber transmission per scattering event Δk_{max} (from Eq. 200):

$$\Delta k_{max}(k, x_1) = k \left(1 - P_{\theta_{max}}(k, x_1) \right), \quad (203)$$

as well as the cross section $d\sigma_{\theta_{max}}$ as a function of $P_{\theta_{max}}$ at maximum scattering angle Eq. 201 inserted into Eq. 195 yields:

$$d\sigma_{\theta_{max}}(k, x_1) = \frac{d\sigma(k, x_1, \theta)}{d\Omega} \Big|_{\theta=\theta_{max}} = \frac{q^4}{4\pi m_{eff}^2} \left(P_{\theta_{max}}(k, x_1) \right)^2. \quad (204)$$

5.3 Estimating the probability of wavenumber transmission

In case of a scattering event, the wavenumber k of the elementary vortex is reduced by Δk . However, this is only valid under the assumption of a free laminar particle as a collision partner. If the environment of the laminar particle is taken into account, local friction can prevent the wavenumber transfer. By briefly evaluating the surroundings of a laminar particle in the boundary layer, the probability of wavenumber transmission can be estimated.

The laminar boundary layer forms a shear flow of layers which slide over one another at different velocities. Relative to a single fluid molecule, which is assumed to be spherical or cylindrical, this situation can be described as shown in Fig. 4b.

In the rest frame of the particle, the upper and lower layers slide over the particle with velocities of $\pm\Delta v$. This sliding motion changes into a rolling motion if the rolling condition is satisfied:

$$\Delta\omega = \frac{\Delta v}{\frac{\sqrt{\pi}}{2}\bar{r}_p} = \frac{4\Delta v}{\sqrt{\pi}d_{box}}, \quad (205)$$

where the stretched dimensionless particle radius $\bar{r}_p = \frac{d_c r_p^{SI}}{l^{SI}}$ was used (d_c is defined according to Eq. 72). The model assumption is therefore that a transfer of angular frequency to the laminar particle only occurs if the local velocity gradient is overcome. In the sphere or cylinder model this means that rolling condition Eq. 205 is fulfilled.

The magnitude of the velocity gradient acting on the particle is decisive in this case. Fortunately, its value has already been estimated by the effective vorticity ω_{eff} (Eq. 86), where the change in velocity over a box is given by:

$$\omega_{eff} = \frac{\partial v}{\partial \bar{x}_2} \approx \frac{2\Delta v}{2\frac{\sqrt{\pi}}{2}\bar{r}_p} = \frac{4\Delta v}{\sqrt{\pi}d_{box}}, \quad (206)$$

which can be directly inserted into rolling condition Eq. 205 and formulated in terms of wave numbers $k = \omega/v$:

$$\Delta k = k_{eff}, \quad (207)$$

with k_{eff} according to Eq. 121. The probability that rolling condition Eq. 207 is satisfied can be determined from two quantities.

First, by the average number of scattering events s needed to transfer the required amount of wavenumber, given by the ratio of required (Eq. 207) to transferred wavenumber (Eq. 200):

$$s(k, x_1, \theta) = \frac{k_{eff.}}{\Delta k(k, x_1, \theta)} = \frac{k_{eff.}}{k(1 - P(k, x_1, \theta))}, \quad (208)$$

and evaluated in the simplified model for the scattering angle with largest momentum transfer θ_{max} (Eq. 203):

$$s_{\theta_{max}}(k, x_1) = s(k, x_1, \theta_{max}) = \frac{k_{eff.}}{k(1 - P_{\theta_{max}}(k, x_1))}. \quad (209)$$

Secondly, by the probability of a scattering event given by the differential cross section $\frac{d\sigma}{d\Omega}$ (Eq. 195). From these two quantities, the probability Φ of a wavenumber transfer can be given as:

$$\Phi(k, x_1, \theta) = \left[\frac{d\sigma(k, x_1, \theta)}{d\Omega} \right]^{s(k, x_1, \theta)}, \quad (210)$$

and again evaluated at θ_{max} (with Eq. 204):

$$\Phi_{\theta_{max}}(k, x_1) = \left[d\sigma_{\theta_{max}}(k, x_1) \right]^{s_{\theta_{max}}(k, x_1)}. \quad (211)$$

5.4 Change of state probability \mathcal{E} amplification

An elementary vortex state $\varepsilon(k)$ is formed when a state with higher wavenumber $\varepsilon(k + \Delta k)$ is subjected to a collision, reducing the wavenumber by Δk . This occurs according to Eq. 211 with a probability of $\Phi_{\theta_{max}}(k + \Delta k, x_1)$. Meanwhile, the resulting state $\varepsilon(k)$ can decay further with probability $\Phi_{\theta_{max}}(k, x_1)$.

For many collisions, this results in a statistical change of the occupation number for state $n'(k, x_1)$, normalized per unit momentum and at a fixed time ($\bar{x}_1 = vt = const.$):

$$n'_{x_1=const}(k, x_1) = \frac{\Phi_{\theta_{max}}(k + \Delta k, x_1) - \Phi_{\theta_{max}}(k, x_1)}{\hbar_{fl}\Delta k} \approx \hbar_{fl}^{-1} \frac{\partial \Phi_{\theta_{max}}(k, x_1)}{\partial k}. \quad (212)$$

I.e. if many scattering processes take place, the occupation number is proportional to the difference between creation and decay probability, which corresponds to the partial derivative of $\Phi_{\theta_{max}}$ with respect to k .

Interpreted classically, this increase in the occupation number corresponds to an amplification of the associated wavenumbers. Thereby, the application of scattering theory ensures the summation over all possible reaction paths.

The initial state of a collision is formed by a laminar particle and an elementary vortex (Fig. 5). The number of expected collisions therefore is proportional to the respective amount fractions c_L and c_ω of these particles per volume considered in position space. The amount fractions are given in the model by Eq. 196. The conversion from

volume in momentum space to position space is done at a fixed time by means of the density of states $D(k)$ (one-dimensional case, no additional degrees of freedom):

$$D(k) = \frac{1}{V^{1d}} \frac{\partial Z_m^{1d}(k)}{\partial k} = \frac{1}{L} \frac{L}{2\pi} = \frac{1}{2\pi d_c}, \quad (213)$$

where the one-dimensional microcanonical partition function without additional degrees of freedom $Z_m^{1d}(k) = \frac{kL}{2\pi}$ was used. The wavenumber-dependent occupation number $n(k, x_1)$ after a distance x_1 of collisions is thus obtained based on the occupation number n' in momentum space (Eq. 212), taking into account the initial concentrations and expressed as density in position space:

$$n(k, x_1) = c_L c_\omega D(k) n'(k, x_1) = \frac{c_L c_\omega}{2\pi d_c \hbar_{fl}} \frac{\partial \Phi_{\theta_{max}}(k, x_1)}{\partial k}. \quad (214)$$

Consequently, if interpreted classically, the occupation number $n(k, x_1)$ according to Eq. 214 corresponds to the amplification factor n for single frequencies of e^N -theory (see e.g. van Ingen 2008 or Simon 2017).

5.4.1 Fluid mechanical interpretation and Schmidt number If in Eq. 214 the fluid action is written out $\hbar_{fl} = \frac{2\pi}{3} (Re_L d_c)^{-1}$ (Eq. 119), an interesting interpretation for the amplification factor emerges:

$$\begin{aligned} n(k, x_1) &= Re_L \frac{3c_L c_\omega}{4\pi^2} \frac{\partial \Phi_{\theta_{max}}(k, x_1)}{\partial k} \\ &= \frac{1}{\nu_L} \frac{3c_L c_\omega}{4\pi^2} \frac{\partial \Phi_{\theta_{max}}(k, x_1)}{\partial k}. \end{aligned} \quad (215)$$

The amplification factor n is inversely proportional to the local, nondimensionalized kinematic viscosity $\nu_L = Re_L^{-1}$ (compare Eq. 4 in Part I). Since at the same time the kinematic viscosity is a measure for possible diffusive momentum transport (momentum diffusivity) (Bergman *et al.*, 2018), the amplification factor can be seen as the ratio between generated momentum and transportable diffusive momentum. For $n > 1$, more momentum is generated than can be diffusively transported. This means that for $n > 1$ convective transport must begin, which together with the internal angular momentum of elementary vortices can lead to convective rotational motion and thus to macroscopic vortex formation.

In this interpretation, however, it is assumed that diffusive momentum transport is equivalent to diffusive mass transport (mass diffusivity). This is usually the case in gases, but does not apply to fluids in general. The measure for the ratio between momentum- and mass-diffusivity in a given fluid is the Schmidt number Sc (Bergman *et al.*, 2018):

$$Sc = \frac{\nu_L}{D}. \quad (216)$$

Where D denotes the nondimensionalized diffusion coefficient for mass diffusivity, and in gases it usually holds that $Sc \approx 1$. For vortex formation, the mass diffusivity should be the decisive quantity, hence the somewhat more general Schmidt-corrected amplification factor n^{Sc} is introduced:

$$n^{Sc}(k, x_1) = Sc \cdot n(k, x_1) = \frac{c_L c_\omega Sc}{2\pi d_c \hbar_{fl}} \frac{\partial \Phi_{\theta_{max}}(k, x_1)}{\partial k}. \quad (217)$$

5.5 Results

5.5.1 Notation and result types The presented model provides two types of results:

First, by calculating Eq. 217, analytical expressions for the amplification factor n , the maximally amplified wavenumber k_{max} , the maximum amplification factor N and the transition point $x_{trans.}$ are given. These expressions are written in the general, nondimensionalized form.

To obtain compact expressions, several terms closely related to the ratio of ingoing vortex to laminar momentum $\frac{\hbar_{fl}k}{m_{eff}}$ are combined as shorthand notations:

$$k_1 = \frac{\hbar_{fl}k}{m_{eff}} = \frac{k}{k_{eff}} = c_2 k \sqrt{x_1}. \quad (218)$$

$$k_2 = 1 + 2k_1 = 1 + 2c_2 k \sqrt{x_1}. \quad (219)$$

$$k_3 = \frac{c_1 k_2 \sqrt{Re_C}}{v \sqrt{c_3 x_1}} = \frac{c_1 (1 + 2c_2 k \sqrt{x_1}) \sqrt{Re_C}}{v \sqrt{c_3 x_1}}. \quad (220)$$

Further short notations and parameters are shown in Table 4. A detailed calculation of the results can be found in the commented *Mathematica* code in the supplementary materials.

Second, two examples with numerical input values are calculated and plotted in Fig. 9. The experimental input values are summarized in Table 5 and are chosen to match the introductory examples in Fig. 2 as closely as possible.

To facilitate comparison with the introductory examples, the nondimensionalized wavenumbers k are converted to frequencies ν^{SI} with dimension. The scaling to dimensionless frequencies is thereby done by the Strouhal number Str (Özgen, 2004; Drazin & Riley, 2006). With the nondimensionalization according to Par. 3.5 and considering the covariant derivative in time direction $v^{-1}\partial_t$ inserted in Eq. 5 in Part I, the following relations are obtained for the dimensionless angular frequency ω and the dimensionless wave number $k = \omega/v$:

$$\omega = 2\pi Str_\infty = \frac{x_1^{SI} \omega^{SI}}{v_\infty^{SI}} \quad \text{and} \quad k = 2\pi Str_L = \frac{x_1^{SI} \omega^{SI}}{v^{SI}}. \quad (221)$$

parameter	symbol	formula	definition
dimensionless inverse velocity profile gradient	c_1	0.332	Eq. 84
coefficient for ratio k_1	c_2	$\frac{d_c v}{c_1 \sqrt{Re_C}}$	Eq. 218
numerical prefactor in the differential cross section	c_3	$\frac{9\pi}{1024}$	Eq. 220
dimensionless box length	d_c	$\frac{d_{box}^{SI}}{2r_p^{SI}}$	Eq. 72
chord Reynolds number	Re_C	$\frac{\rho^{SI} v_\infty^{SI} l_c^{SI}}{\mu^{SI}}$	Eq. 122
dimensionless velocity along scattering profile	v	0.220	Eq. 199

Table 4: Shorthand notations and parameters used in this section. Dimensional quantities are marked with a superscript $()^{SI}$.

input quantity	symbol	wind tunnel	test flight	unit
freestream velocity	v_∞^{SI}	14	41	m/s
dyn. viscosity	η^{SI}	$19.6 \cdot 10^{-6}$	$14.9 \cdot 10^{-6}$	Pa · s
chord length ^a	l_c^{SI}	1	1.35	m
density ^b	ρ_∞^{SI}	1.225	1.007	kg/m ³
mean free path ^{b,c}	d_{box}^{SI}	$67 \cdot 10^{-9}$	$81 \cdot 10^{-9}$	m
mean radius of an air particle ^c	r_p^{SI}	$0.182 \cdot 10^{-9}$	$0.182 \cdot 10^{-9}$	m
const. wave number for k_3^0	k^0	250	250	–
const. distance for k_3^0	x_1^0	0.6	0.6	–
Schmidt number	Sc	1	1	–

Table 5: Numerical input values used in the calculation of the examples.

^a Since l_c^{SI} acts as a scaling factor of the x_1 axis, inserting $l_c^{SI} = 1$ m corresponds to an unscaled representation. ^b Numerical values are estimated for standard atmosphere at 0 m.a.s.l. (wind tunnel) and 2'000 m.a.s.l. (flight). (EngineeringToolBox, 2003; Czernia, 2022). ^c Kinetic radius of nitrogen N₂ (Ismail, Khulbe & Matsuura, 2015).

Thereby, $v^{SI} = v v_\infty^{SI}$ denotes the dimensional local velocity, Sr_∞ the Strouhal number at infinite distance from the plate, and Sr_L the local Strouhal number:

$$Sr_\infty = \frac{x_1^{SI} \nu^{SI}}{v_\infty^{SI}} \quad \text{and} \quad Sr_L = \frac{x_1^{SI} \nu^{SI}}{v^{SI}}. \quad (222)$$

The substitution to the dimensional frequency ν^{SI} is thus given by:

$$k \rightarrow \frac{2\pi x_1^{SI}}{v^{SI}} \nu^{SI}. \quad (223)$$

5.5.2 Amplification factor n^{Sc} The amplification factor is determined by substituting Eq. 211 into Eq. 217 and yields with the shortcuts introduced in Par. 5.5.1:

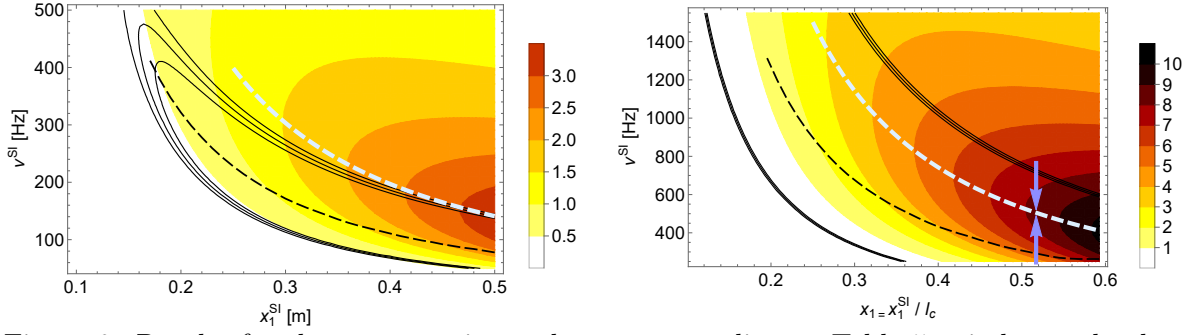


Figure 9: Results for the two experimental setups according to Table 5, wind tunnel values on the left and test flight values on the right. The amplification factor n^{Sc} is depicted using yellow-red-black contours, the maximum amplified frequency ν_{max}^{SI} is superimposed with the light blue dashed line. The two vertical arrows in the flight example denote the transition point x_{trans}^{Sc} at $N_{trans.} = 9$. For comparison with the introductory examples in Fig. 2, the instability zones are indicated using black contours, where the contours are plotted at function values $\{9, 9.5, 10\}$. The instability maximum (black dashed line) is determined numerically and applied for comparison.

$$n^{Sc}(k, x_1) = \frac{3c_1 c_L c_\omega Re_C^{3/2} Sc \sqrt{x_1}}{2\pi^2 d_c} \frac{1}{k^2} k_3^{-s_{\theta_{max}}} \left[-1 + (k_1^{-1} + 1) \ln(k_3) \right]. \quad (224)$$

As a function of dimensional quantities to visualize the numerical examples, the amplification factor reads (substitution according to Eq. 223):

$$n^{Sc}(\nu^{SI}, x_1) = \frac{3c_1 c_L c_\omega Re_C^{3/2} (\nu^{SI})^2 Sc}{8\pi^4 d_c (l_c^{SI})^2} (\nu^{SI})^{-2} x_1^{-3/2} k_3^{-s_{\theta_{max}}} \left[-1 + (k_1^{-1} + 1) \ln(k_3) \right]. \quad (225)$$

The amplification factor according to Eq. 225 is plotted using yellow-red-black contours for the two experimental setups according to Table 5 in Fig. 9.

5.5.3 Approximation for the calculation of the maximum amplified wavenumber and the transition point In the case where ratio k_1 (Eq. 218) between wavenumbers of incoming elementary vortices and the velocity gradient is large, an analytical expression can be given for the maximum amplified wavenumber k_{max} as a function of x_1 . The approximation for large k_1 involves three components:

- The ratio is sufficiently large, i.e. $k_1 = \frac{k}{k_{eff}} = c_2 k \sqrt{x_1} \gg \frac{3}{2}$.
- This causes the logarithm $\ln(k_3)$ in Eq. 224 to be sufficiently large, namely $\ln(k_3) \gg 3$.
- In addition, this logarithm only changes marginally in the range considered, which allows it to be assumed constant, $\ln(k_3) \approx const$. This is introduced by substituting

a constant k_3^0 in place of k_3 :

$$\ln(k_3) \rightarrow \ln(k_3^0) \quad \text{with} \quad k_3^0 = \frac{c_1(1 + 2c_2k^0\sqrt{x_1^0})\sqrt{Re_C}}{v\sqrt{c_3x_1^0}}. \quad (226)$$

Thereby, the k - and x_1 -dependency within the logarithm is replaced by constant terms k^0 and x_1^0 , which allows the sought expressions to be resolved for k and x_1 . The constant terms are listed in Table 5 and are chosen to be in the range of transition. As requested, the dependence of the numerical results on these parameters is weak, but they may need to be adjusted for different fluids.

5.5.4 Approximated max. amplified wavenumber k_{max} and frequency ν_{max}^{SI} The maximum amplified wavenumber k_{max} at fixed coordinate x_1 is found by zeroing the partial derivative of the amplification factor (Eq. 224) according to $\partial n^{Sc}(k, x_1)/\partial k = 0$, with the result:

$$k_{max}(x_1) \underset{k_1 \gg \frac{3}{2}}{\approx} \frac{c_1 \ln(k_3^0) \sqrt{Re_C}}{d_c v} x_1^{-1/2}, \quad (227)$$

where the approximation from Par. 5.5.3 was applied. The maximum amplified dimensional frequency ν_{max}^{SI} is given accordingly (substitution as per Eq. 223):

$$\nu_{max}^{SI}(x_1) \underset{k_1 \gg \frac{3}{2}}{\approx} \frac{c_1 \ln(k_3^0) \sqrt{Re_C} v_\infty^{SI}}{2\pi d_c l_c^{SI}} x_1^{-3/2}. \quad (228)$$

The maximum amplified frequency Eq. 228 is displayed in Fig. 9 with the light blue dashed line. For the specific wind tunnel (*wt*) and flight examples, simplified formulae for this curve can be given by inserting some of the numerical quantities of weak dependency:

$$\begin{aligned} k_{max}^{wt}(x_1) &\approx 0.109 \sqrt{Re_C} x_1^{-1/2} \\ k_{max}^{flight}(x_1) &\approx 0.0912 \sqrt{Re_C} x_1^{-1/2}, \end{aligned} \quad (229)$$

as well as with dimensional units:

$$\begin{aligned} \nu_{max}^{SI,wt}(x_1) &\approx \frac{0.0038 \sqrt{Re_C} v_\infty^{SI}}{l_c^{SI}} x_1^{-3/2} \\ \nu_{max}^{SI,flight}(x_1) &\approx \frac{0.00319 \sqrt{Re_C} v_\infty^{SI}}{l_c^{SI}} x_1^{-3/2}. \end{aligned} \quad (230)$$

5.5.5 Approximated max. amplification factor N^{Sc} Substituting the maximum amplified wavenumber Eq. 227 into the amplification factor Eq. 224 yields the maximum amplification factor N as a function of the position coordinate:

$$N^{Sc}(x_1) \underset{k_1 \gg \frac{3}{2}}{\approx} \frac{3 \cdot c_L c_\omega d_c Re_C Sc v x_1}{\sqrt{c_3} \pi^2} \left(\frac{v \sqrt{c_3 x_1}}{2c_1 \sqrt{Re_C} \ln k_3^0} \right)^{\frac{2 + \ln k_3^0}{\ln k_3^0}}. \quad (231)$$

The maximum amplification factor N^{Sc} according to Eq. 231 represents the magnitude of the amplification factor n on the light blue dashed line defined by the maximum amplified frequency ν_{max}^{SI} in Fig. 9. At the same time, it corresponds to the N factor in e^N -theory.

The simplified formulae for the amplification factor with parameters inserted are as follows for the two examples:

$$\begin{aligned} N_{wt}^{Sc}(x_1) &\approx 0.0336 Re_C^{0.424} x_1^{1.58} \\ N_{flight}^{Sc}(x_1) &\approx 0.0405 Re_C^{0.426} x_1^{1.57}. \end{aligned} \quad (232)$$

5.5.6 Approximated transition point $x_{trans.}^{Sc}$. The transition point $x_{trans.}^{Sc}$ is determined by the maximum amplification factor N exceeding a certain numerical value $N_{trans.}$. Usually, it is set to e.g. $N_{trans.} = 9$. This is substituted into Eq. 231:

$$N_{trans.} = N^{Sc}(x_{trans.}^{Sc}), \quad (233)$$

and resolving to $x_{trans.}^{Sc}$ gives the transition point:

$$x_{trans.}^{Sc}(N_{trans.}) \underset{k_1 \gg \frac{3}{2}}{\approx} Re_C^{\frac{2 - \ln k_3^0}{2 + 3 \ln k_3^0}} \left[\frac{2c_1 \pi^2 N_{trans.} \ln(k_3^0)}{3c_L c_\omega d_c Sc v^2} \left(\frac{2c_1 \ln(k_3^0)}{\sqrt{c_3} v} \right)^{\frac{2}{\ln k_3^0}} \right]^{\frac{2 \ln k_3^0}{2 + 3 \ln k_3^0}}. \quad (234)$$

$x_{trans.}^{Sc}$ corresponds to the nondimensionalized coordinate. The transition point $x_{trans.}^{Sc}$ with $N_{trans.} = 9$ is illustrated in Fig. 9 by the two vertical arrows, which are drawn at the level of the maximum amplified frequency.

In both examples, the transition point with the numeric parameters inserted can be expressed as:

$$\begin{aligned} x_{trans.}^{Sc, wt}(N_{trans.}) &\approx 8.61 N_{trans.}^{0.635} Re_C^{-0.269} = 0.870 \text{ m} \\ x_{trans.}^{Sc, flight}(N_{trans.}) &\approx 7.67 N_{trans.}^{0.635} Re_C^{-0.270} = 0.698 \text{ m} = 0.517 l_c^{SI}. \end{aligned} \quad (235)$$

The approximated formula results in the determined transition point being slightly shifted upstream compared to the actual contour $N = 9$ as given by the original amplification factor n^{Sc} .

5.5.7 Instability zone The instability zone I^{Sc} is determined by partial derivative of the state amplification factor Eq. 225 with respect to x_1 :

$$I^{Sc}(\nu^{SI}, x_1) = \frac{\partial n^{Sc}(\nu^{SI}, x_1)}{\partial x_1}. \quad (236)$$

This is indicated by the black contours in Fig. 9, where the contours are plotted at function values $\{9, 9.5, 10\}$. The maximum instability (black dashed line in Fig. 9) is determined numerically and added for comparison with the introductory examples.

6 Conclusion

6.1 Summary

In Part I, a method is presented to locally diagonalize the strain-rate tensor of viscous fluids in turbulent flows.

To symmetrize the tensor, a local polar decomposition approach is introduced, generating a $U(1)$ gauge field. For diagonalization, $SO(3)$ rotating fields are used to transform into the respective local eigensystem.

By applying the constitutive equation, a corresponding stress tensor field is derived and by calculating its gradient, the local fields are identified and interpreted as velocity field components of the Navier-Stokes equations (NS equations).

It is shown that the novel field equation contains all the information of the steady-state NS equations up to a global similarity transformation, with the information on the diffusive flow components included in the locally diagonalized part, while the information on the nonlinear convective components is incorporated by the gauge fields. The nonlinearity is further structured in the self-interaction terms of the $SO(3)$ fields. The $U(1)$ field contains the compressibility effects.

In Part II this fundamental theory is developed to the point where a basic example can be computed as a proof-of-concept. For this purpose, the field equation from Part I is brought into a form in which the path integral formalism can be applied. In particular, the step from the description as a steady flow to a scattering theory with covariant time evolution using Wick rotation is performed and analyzed in detail.

In the course of the argument, the equation is considerably simplified for a two-dimensional incompressible flow, which reduces the gauge fields to a single, abelian $U(1)$ field. For this situation, a first scattering theory is formulated.

Based on this, a model using the scattering of quasiparticles among each other to mechanistically explain the formation of TS waves in the boundary flow over a flat plate is presented. The quasiparticles are modeled as average air molecules, which either travel primarily vortex-free (laminar particles), or are characterized by high inherent angular momentum (elementary vortices). The inherent angular momentum is characterized by a wavenumber. The mechanism of the model includes the following steps:

- (i) Generation of elementary vortices upon impact on the leading edge of the plate.
- (ii) Scattering of elementary vortices on laminar particles within the boundary layer, thereby reducing the wavenumber of the elementary vortices during impact. This reduction is more pronounced at high wavenumbers and is reduced at low wavenumbers.

- (iii) Repeated impacts result in an accumulation of elementary vortices of certain wavenumbers, which leads to superposition, amplification and emergence of macroscopic vortices.

As a result, an analytical solution is given for the maximum amplified wavenumbers and frequencies as well as for the transition point from laminar to turbulent flow. The model is applied to two specific flow situations, and the corresponding numerical results are calculated.

6.2 Discussion of the local gauge field approach

The goal of this manuscript is to formulate fluid mechanics as a local gauge field theory and to show how this new perspective can be applied advantageously.

This goal is achieved: A local gauge field equation for fluids is derived from elementary physical relations and it is shown that this equation contains the equivalent information to the stationary Navier-Stokes equations in situations of perturbed stationary flows and up to a global similarity transformation.

Furthermore, it is demonstrated how a scattering theory can be developed from this gauge field equation and applied to a relevant problem in fluid mechanics. Thus, a proof of concept is achieved for the application of scattering theories and the path integral formalism in flow situations. Two fundamental advantages of the new approach become apparent:

- (i) The gauge fields partition and structure the complex information of a turbulent flow pattern to a great extent. Convective and diffusive parts are separated, the nonlinearity is structured by the self-interaction of the non-Abelian $SO(3)$ -fields. A variety of mathematical methods from Yang-Mills theory are available to treat the arising terms.
- (ii) The new approach offers advantages when it becomes impossible to follow the path of individual fluid volumina along streamlines due to chaotic motion. The approach through path integral formalism processes all information about all possible trajectories and reaction pathways as well as their probability at the same time. As a result, it directly provides a statistical evaluation of the flow's characteristics, and may produce analytical formulae and results that are otherwise unattainable or are achievable by numerical calculation only.

Discussion of the dynamic aspects: The Wick rotation initially introduces a relativistically covariant time evolution. This effectively gives the wave functions the actual form of wave packets $\psi^0 \propto \mathbf{A}e^{i(\omega t - k_1 x^1)}$ (see Eq. 139). They can thus be viewed as local, dynamical wave-like perturbations, as used in traditional e^N methods, allowing the treatment of dynamical problems such as the emergence of TS waves and turbulence.

Through the solution mechanism as a path integral, the dynamic contributions are subsequently integrated out and the solutions contain only stationary components.

In this sense, the new approach extracts the stationary aspects of the flow, which are obtained through statistical averaging over all possible paths.

Discussion of the solutions regarding $\dot{\epsilon}^C$: To achieve a consistent treatment of the phase field, a global transformation is added in Par. 2.2.3 to the strain-rate tensor to become $\dot{\epsilon} \rightarrow \dot{\epsilon}^C = i\sigma^2 \dot{\epsilon}$. As a result, a Dirac-like equation for the fluid wave function ψ^α is derived and processed. However, for problems without phase dependency (e.g. incompressible flows), it may be easier to solve the non-transformed Eq. 11 directly, without modification of the strain-rate-tensor $\dot{\epsilon}$.

This equation has the principal form of a Lagrangian to the Euclidean Majorana equation (see van Nieuwenhuizen & Waldron 1996) and can be developed accordingly to a Majorana-based scattering theory (with the corresponding restrictions concerning reality condition). The important point for this work is that the connection between the two equations is well-known and well-studied (see, for example, Anastasiou 2020 or the discussion in Phibert, JamalS & Abdulkhakimov 2014). Thus, despite solving the modified system with respect to $\dot{\epsilon}^C$, the original strain-rate tensor can be constructed from the obtained solutions if needed.

6.3 Discussion of the Tollmien-Schlichting model

While the derivation of the scattering theory for fluids is kept as general as possible, a number of approximations and simplifications are introduced when modeling the process of wave generation for the Tollmien-Schlichting examples (TS-model). These approximations must be assessed and validated separately from the underlying theory. In summary, the assumptions are:

- The flow is two-dimensional and incompressible.
- There is a disturbance which generates and distributes vortex particles (presented assumption: Point disturbance by tip of plate; distribution by diffusion).
- Only contributions in first order perturbation theory are included.
- Only those scattering processes are considered which cause the largest momentum transfer.
- The air/ fluid molecules can be approximated as cylindrical particles with averaged size and spacing.
- Only scattering processes at the height of momentum thickness δ_2 are considered.
- There is a lower limit for angular momentum transfer in the scattering process (presented assumption: A rolling condition imposed by the velocity gradient must be satisfied).

Within these assumptions, the TS-model provides a detailed step-by-step mechanism for the emergence of turbulence on a microscopic basis.

Comparison with traditional methods (e^N etc.) reveals some interesting aspects:

- The model calculation is analytically feasible and much simpler than numerical calculation methods involving fourth-order differential equations, which are used in e^N -approaches.
- In contrast to numerical results, the analytical solution makes it possible to further investigate and possibly improve the understanding of influencing factors on the generation of turbulence.
- Compared to e^N -methods, calibration difficulties are omitted, which occur when adjusting the computational method (van Ingen, 2008) or environmental conditions (Reeh, 2014).

The correlation of the newly calculated results with the original examples is agreeable. In summary, however, this initial, basic TS-model is probably too simplistic for detailed quantitative analysis. Nonetheless, it does demonstrate qualitatively interesting features – such as the characteristic “banana” shape of the instability zone – and the basic feasibility and usefulness of a scattering theory for problems in fluid mechanics, which is consistent with the primary goal of this article in the form of a proof-of-concept.

6.4 Outlook

In this article, a basic theory is established and its general usefulness was demonstrated in a simple situation. However, there are many areas which deserve to be investigated further:

Comparison to experimental findings: The calculation has so far only been compared to two theoretical calculations. A possible next step is to compare the model results with actual measurements. On one hand, it can be clarified to what extent quantitatively accurate results can be generated with the model. On the other hand, an investigation of the proposed contributing factors outside Reynolds theory (such as the size and spacing of the fluid molecules, possibly their shape) may also be interesting.

Then, the question whether the model can be used or adapted to other fluids and situations should be investigated. In particular, flows in pipes are another possible application.

Further development of the theory within fluid mechanics: The tool developed is not restricted to TS waves, but can possibly be used to model further effects in the transition to turbulent flow. In principle, three-dimensional flows as well as terms of higher order including self-interaction should be considered, categorized and systematized.

As an exemplary idea, higher order interactions may limit the lifetime of vortices, which can be used to form an analytical model for localized puffs in the transition to turbulence. However, such concepts first require a formulation of the full, non-abelian scattering theory including perturbations of higher order.

Using the approach in different domains: The gauge field equation presented in this manuscript can be applied virtually without change to elastic media. They obey the same general mechanics as the Cauchy-momentum equations (Eq. 5 in Part I), but in this case inserting an elastic constitutive equation (roughly $\boldsymbol{\sigma} \propto \boldsymbol{\varepsilon}$), with $\boldsymbol{\varepsilon}$ denoting the strain tensor. Mathematically this system is equivalent to a fluid, the only significant difference lies in its physical interpretation.

Acknowledgments

My thanks go to Rudolf Fehlmann for the countless, fruitful discussions and in particular for his support in the structuring of my work. Likewise, my thanks go to my sister Charlotte Merz for her help in language editing, as well as to everyone else surrounding me, my family and friends, for the ongoing support.

Declaration of Interests: None.

References

- W. Tollmien, Über die Entstehung der Turbulenz. 1. Mitteilung. *Nachrichten von der Gesellschaft der Wissenschaften zu Göttingen, Mathematisch-Physikalische Klasse* **1929**, 21-44. [Link]
- H. Schlichting, Zur Entstehung der Turbulenz bei der Plattenströmung. *Nachrichten von der Gesellschaft der Wissenschaften zu Göttingen, Mathematisch-Physikalische Klasse* **1933**, 181-208. [Link]
- H. Schlichting and K. Gersten. *Boundary-Layer Theory*; Springer, 2017; ISBN 978-3-662-52917-1; doi:10.1007/978-3-662-52919-5. [Link]
- J.L. van Ingen, The e^N method for transition prediction. Historical review of work at TU Delft. *Proceedings of the 38th AIAA Fluid Dynamics Conference and Exhibit* **2008**, 1-49; doi:10.2514/6.2008-3830. [Link]
- P.J. Schmid and D.S. Henningson. *Stability and transition in shear flows*; Springer, 2012; ISBN 978-0-387-98985-3; doi:10.1007/978-1-4613-0185-1. [Link]
- B.J. Simon. *Active Cancellation of Tollmien-Schlichting Waves under Varying Inflow Conditions for In-Flight Application*; Technische Universität Darmstadt, Fachbereich Maschinenbau, 2017. [Link]
- A.D. Reeh. *Natural Laminar Flow Airfoil Behavior in Cruise Flight through Atmospheric Turbulence*; Technische Universität Darmstadt, Fachbereich Maschinenbau, 2014. [Link]
- P. Renaud. *Clifford algebras lecture notes on applications in physics*; University of Canterbury: Christchurch, NZ, 2022; HAL Id: hal-03015551. [Link]
- W.O. Straub. *A Child's Guide to Spinors*; Pasadena, CA, 2016. [Link]
- H. Blasius, Grenzsichten in Flüssigkeiten mit kleiner Reibung. *Z. Angew. Math. Phys.* **1908**, 56, 1-37.
- M.K. Jaman and M.R. Molla and S. Sultana, Numerical Approximations of Blasius Boundary Layer Equation. *Univ.J.Sci.* **2011**, 59(1), 87-90. [Link]
- P. van Nieuwenhuizen and A. Waldron, On Euclidean spinors and Wick rotations. *Physics Letters B* **1996**, 389(1), 29-36; doi:10.48550/arXiv.hep-th/9608174. [Link]
- S. Friedli and Y. Velenik. *Statistical Mechanics of Lattice Systems: A Concrete Mathematical Introduction - Ch.10 Reflection Positivity*; Cambridge University Press, 2017; ISBN 978-1-107-18482-4; doi:10.1017/9781316882603. [Link]
- K.-H. Neeb, G. Ólafsson, Reflection Positivity – A Representation Theoretic Perspective. *arXiv* **2018**; doi:10.48550/arXiv.1802.09037. [Link]

- K. Osterwalder and R. Schrader, Axioms for Euclidean Green's functions. *Comm. Math. Phys.* **1973**, 31, 83–112. [Link]
- K. Osterwalder and R. Schrader, Axioms for Euclidean Green's functions II. *Comm. Math. Phys.* **1973**, 42, 281–305. [Link]
- G.C. Wick, Properties of Bethe-Salpeter Wave Functions. *Physical Review* **1954**, 96(4), 1124–1134; doi:10.1103/PhysRev.96.1124. [Link]
- B.F. Rizzuti and G.F. Vasconcelos Júnior and M.A. Resende, To square root the Lagrangian or not: an underlying geometrical analysis on classical and relativistic mechanical models. *arXiv* **2019**; doi:10.48550/arxiv.1905.01177. [Link]
- C. Burgess and G. Moore. *The Standard Model: A Primer*; Cambridge University Press, 2006; doi:10.1017/CBO9780511819698. [Link]
- M.E. Peskin and D.V. Schroeder. *An Introduction To Quantum Field Theory*; CRC Press, 1995; doi:doi:10.1201/9780429503559. [Link]
- V. Chiochia and G. Dissertori and T. Gehrmann. *Phenomenology of Particle Physics I*; ETH Zurich and University of Zurich, 2010. [Link]
- A. Lawson. *Compton Scattering from Quantum Electrodynamics*; University of Southampton, 2014. [Link]
- D. Millar. *A Calculation of the Differential Cross Section for Compton Scattering in Tree-Level Quantum Electrodynamics*; University of Southampton, 2014. [Link]
- Y. Friedman, Representations of the Poincaré group on relativistic phase space. *arXiv* **2008**; doi:10.48550/arxiv.0802.0070. [Link]
- C. Anastasiou. *Quantum Field Theory I*; ETH Zurich, 2020. [Link]
- Phibert and JamalS and M. Abdukhakimov, *Dirac, Weyl and Majorana Spinors* **2014**; Physics Stack Exchange available at: <https://physics.stackexchange.com/questions/103005/dirac-weyl-and-majorana-spinors>; accessed 19.6.2022. [Link]
- T.L. Bergman and A.S. Lavine and F.P. Incropera and D.P. DeWitt. *Fundamentals of Heat and Mass Transfer, 8th Edition*; Wiley, 2018; ISBN 978-1-119-35388-1. [Link]
- Engineering ToolBox, *U.S. Standard Atmosphere vs. Altitude* **2003**; available at: https://www.engineeringtoolbox.com/standard-atmosphere-d_604.html; accessed 22.5.2022. [Link]
- D. Czernia, *Mean Free Path Calculator* **2022**; available at: <https://www.omnicalculator.com/physics/mean-free-path>; accessed 22.5.2022. [Link]
- A.F. Ismail and K.C. Khulbe and T. Matsuura. *Gas Separation Membranes: Polymeric and Inorganic*; Springer, 2015; ISBN 978-3-319-01095-3; doi:10.1007/978-3-319-01095-3. [Link]
- S. Özgen, Effect of heat transfer on stability and transition characteristics of boundary-layers. *International Journal of Heat and Mass Transfer* **2004**, 47(22), 4697–4712; doi:10.1016/j.ijheatmasstransfer.2004.05.026. [Link]
- P. Drazin and N. Riley. *The Navier-Stokes Equations: A Classification of Flows and Exact Solutions*; Cambridge University Press, 2006; ISBN 978-0-511-52645-9; doi:10.1017/CBO9780511526459. [Link]